Ecological Modelling 468 (2022) 109907

Contents lists available at ScienceDirect

Ecological Modelling

journal homepage: www.elsevier.com/locate/ecolmodel

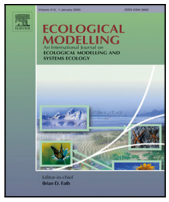

Controls and characteristics of biomass quantization in size-structured planktonic ecosystem models

Jordyn E. Moscoso *, Daniele Bianchi, Andrew L. Stewart

Department of Atmospheric and Oceanic Sciences, Maths Science Building, 520 Portola Plaza, Los Angeles, CA 90095, United States of America

ARTICLE INFO

Keywords:
Marine phytoplankton
Marine zooplankton
Size spectra

ABSTRACT

Strong relationships between size and other traits have long motivated studies of the size structure and dynamics of planktonic food webs. Size structured ecosystem models (SSEMs) are often used to represent the behavior of these ecosystems, with organism size as a first order approximation of the axis of biological diversity. Previous studies using SSEMs have reported the emergence of localized "peaks" in the size spectrum, a phenomenon that will be referred to in this study as "quantization". However, SSEMs that are used routinely in Earth System Models (ESMs), they tend to be too coarsely discretized to resolve quantization. Observational studies of plankton biomass have also shown qualitatively similar patterns, with localized peaks along the size spectrum. The conditions under which quantization occurs and the ecosystem parameters that control the locations of the biomass "peaks" along the size spectrum have not been systematically explored. This study serves to simultaneously advance our understanding of the constraints on quantization in size-structured ecosystems, and to suggest an approach to discretizing SSEMs that leverages quantization to select a greatly reduced number of size classes. A size-structured model of the pelagic food web, similar to those implemented in global models, is used to investigate the sensitivity of biomass peaks to predator–prey interactions, and nutrient forcing. This study shows that the location of biomass peaks along the size spectrum is strongly controlled by the size selectivity of predation, and the location of biomass peaks along the size spectrum is less sensitive to variations in nutrient supply, external ecosystem forcing, and vertical heterogeneity. Taking advantage of a robust localization of biomass peaks, the dynamics of a continuous planktonic size spectrum to be represented using a few selected size classes, corresponding to locations of the peaks along the size spectrum. These findings offer an insight on how to approach discretization of size structured ecosystem model in Earth system models.

1. Introduction

Phytoplankton form the base of the marine food-web, and understanding their community structure can aid in predicting the composition and productivity of higher trophic levels and top predators (Stock et al., 2017). Community composition depends on complex interactions between the physical environment, resource availability, competition, and predation, which in turn determine patterns of productivity (Hutchinson, 1961; Hillebrand and Azovsky, 2001; Righetti et al., 2019; Mousing et al., 2016; Steele and Henderson, 1992; Vallina et al., 2014).

Numerical and theoretical models have long been used as a tool to understand plankton behavior and interactions in the context of physical drivers, ecology, and food-web dynamics (Armstrong and McGehee, 1980; Follows and Dutkiewicz, 2011; Adjou et al., 2012; Ward et al., 2014; Lévy et al., 2014). However, models often lack levels of diversity found in oceanic plankton communities (Loeuille and Loreau, 2005). Instead of explicitly capturing large-scale biodiversity, specific ecological and functional traits are often chosen to represent planktonic diversity in models (Follows and Dutkiewicz, 2011). Size has long been used to model planktonic diversity (Moloney and Field, 1991; Poulin and Franks, 2010; Banas, 2011; Ward et al., 2012; Sauterey et al., 2017) because of strong empirical relationships between size and other physiological and ecological traits (Andersen et al., 2016; Litchman et al., 2007). More broadly, size mechanistically controls a variety of ecological processes, from resource uptake strategies, to predator–prey interactions across trophic levels (Andersen et al., 2016).

The distribution of dominant phytoplankton sizes is, broadly speaking, a function of resource availability and predation, i.e., bottom-up and top-down processes (McQueen et al., 1986; Lehman, 1991; Banse, 1994; Verity and Smetacek, 1996; Chenillat et al., 2013). In oligotrophic environments, small cells are responsible for most of the

* Corresponding author.
E-mail address: jmoscoso@atmos.ucla.edu (J.E. Moscoso).

https://doi.org/10.1016/j.ecolmodel.2022.109907
Received 29 June 2021; Received in revised form 8 December 2021; Accepted 10 February 2022
Available online 6 April 2022

total phytoplankton biomass (Chisholm, 1992; Partensky et al., 1999; Worden et al., 2004). In contrast, in productive regions, characterized by high chlorophyll and nutrient concentrations, large cells are responsible for a substantial fraction of phytoplankton blooms and biomass variability (Chavez, 1989; Chisholm, 1992; Cavender-Bares et al., 2001; Venrick, 2002). Ecosystems that are dominated by low levels of surface nutrients and small phytoplankton size are characterized by fast nutrient cycling near the surface (Fowler et al., 2020; Partensky et al., 1999). This is a consequence of rapid uptake rates and strong grazing pressures (Tang, 1995). In contrast, ecosystems with high levels of surface nutrients and large phytoplankton size are characterized by weak recycling at the surface and significant export of sinking organic matter, supporting the oceanic carbon pump (Tréguer et al., 2018; Boyd et al., 2019). Large phytoplankton require more macro-nutrients and are usually characterized by larger half saturation constants, and hence slower uptake rates, compared to smaller organisms. However, they benefit from lower grazing pressure as a consequence of their size (Tang, 1995; Hansen et al., 1994), especially during bloom conditions (Behrenfeld and Boss, 2014). Zooplankton follow patterns of food uptake and limitation as a function of size that are similar to phytoplankton (Hansen et al., 1994). Small zooplankton tend to quickly graze small phytoplankton, whereas large zooplankton grazing rates are often outpaced by large phytoplankton, allowing for the prevalence of large phytoplankton species in nutrient-rich regions (Fuchs and Franks, 2010; Ingrid et al., 1996; Leibold, 1996). This phenomenon favors growth of intermediate and large phytoplankton, even with slower uptake rates relative to their smaller counterparts (Terseleer et al., 2014).

Previous observational studies of ecosystem dynamics have shown that phytoplankton size and total biomass follow a power-law size spectrum with small phytoplankton contributing to a large percentage of the biomass (Partensky et al., 1999; Franks, 2002; Zhou and Huntley, 1997). Sheldon et al. (1972) extended this spectrum to suggest a universal power-law relationship for ocean food-webs between the size of an organism and its standing biomass stock. However, simple power-law relationships have been shown to break down in regions with high nutrient concentrations (e.g., coastal margins) (Hood et al., 1991; Huete-Ortega et al., 2014; Jonasz and Fournier, 1996; Schartau et al., 2010; Worden et al., 2004; Zubkov et al., 2000), which show intermediate peaks in biomass along the size spectrum that tend to aggregate around specific phytoplankton sizes (Cavender-Bares et al., 2001; Karp-Boss et al., 2007; Giometto et al., 2013). We refer to this phenomenon as "quantization" of the phytoplankton size spectrum.

Quantization in plankton size spectra has been previously captured and reported in numerical models (Banas, 2011; Sauterey et al., 2017). Trait-based models like size structured ecosystem models (SSEMs) allow for increased understanding of planktonic dynamics in the context of resource competition (Huisman and Weissing, 2001; Follows and Dutkiewicz, 2011). The choice to model dynamics with respect to size can lead to quantization in biomass (Loeuille and Loreau, 2005), and has been shown to be affected by the functional formulation of grazing (Banas, 2011). Specifically, Banas (2011) note that varying the width of the "window" of phytoplankton sizes that can be grazed by a given zooplankton size class changes the number of quantized "peaks" that emerge in the resulting biomass size spectra. A smaller grazing window, corresponding to more specialized zooplankton grazing, allows the coexistence of a larger number of size peaks in the phytoplankton and zooplankton size spectrum. Furthermore, in ecosystem models where each zooplankton size class grazes only a single phytoplankton size class, i.e. when grazing is extremely selective, quantization does not occur (e.g. Franks (2002)). Size structured ecosystem models of higher complexity, such as that presented by Ward et al. (2012), show that while small phytoplankton are always globally present, in agreement with observations, larger phytoplankton are generally found in regions with high nutrient concentrations, such as near continental margins. However, this model does not show size quantization, likely because of the relatively coarse resolution of phytoplankton size spectra. Thus, it remains unclear to what extent quantization is a robust feature of size-structured ecosystems, and what factors determine its emergence and characteristics under typical oceanic conditions.

In this study, we investigate size quantization in a minimal complexity size-structured nutrient, phytoplankton, zooplankton, detritus (NPZD) model, similar to models used in previous work (Banas, 2011; Ward et al., 2012). We run a series of experiments to understand how the model parameters control quantization and the location of the biomass peaks along the size spectrum in both zero- and one-dimensional (0D and 1D) environments. We identify a few salient parameters that have been shown previously to be important in capturing ecosystem dynamics, these include the nutrient supply (Sarmiento and Gruber, 2006), the grazing profile and preference (Banas, 2011; Chenillat et al., 2021), and size resolution as a proxy of diversity, Henson et al. (2021). As a consequence of robust quantization in the solutions presented in the following sections, we are able to propose a reduction in order in size space, and suggest that planktonic ecosystems can be effectively modeled using a small number of representative size classes, providing additional theoretical support for a widespread practice in ecosystem modeling.

The rest of the paper is organized as follows: In Section 2, we describe the size structured ecosystem model. In Section 3, we investigate the impacts of top-down and bottom-up controls on planktonic size spectra through a series of experiments that explore the ecosystem response to change in grazing strategies and nutrient supply, respectively. In Section 4, we show that quantization is robust in 1D, and that relationships between top-down and bottom-up control found in 0D generalize to 1D solutions. In Section 5, we take advantage of robust quantization in 0D and 1D and demonstrate a method in which SSEMs can be reduced to a few carefully chosen size classes that represent the planktonic ecosystem when a large number of phytoplantkon size classes are not feasible to use (eg. in high resolution regional models or ESMs). Finally, in Section 6 we discuss the results and conclude the paper.

2. Size-structured ecosystem model

2.1. Model rationale

We use a size structured ecosystem model based on those developed by Banas (2011) and Ward et al. (2012), and representative of commonly used size-structured models (Armstrong, 1994; Poulin and Franks, 2010; Follows et al., 2007; Dutkiewicz et al., 2012). Size is the primary axis of diversity, reflecting robust allometric relationship between an organisms size and resource encounter strategies (e.g. nutrient acquisition and grazing) (Follows et al., 2007; Litchman et al., 2007; Tang, 1995; Eppley et al., 1969; Hansen et al., 1994; Klausmeier et al., 2020). Using individual size as the axis of diversity can further reduce the dimensionality of the model's parameter space (Follows and Dutkiewicz, 2011). While plankton diversity has been thought to be sustained by niche selection and trait adaption (Hutchinson, 1961; Sommer, 1989), modeled planktonic ecosystems have been shown to collapse to a few representative groups as a consequence of competition, Sauterey et al. (2017), Banas (2011), Loeuille and Loreau (2005) even with models that simulate many species (Merico et al., 2014; Bruggeman and Kooijman, 2007; Follows et al., 2007). Therefore, we use a single functional axis of diversity in size as the basis for our ecosystem model. Aspects of the model such as nutrient uptake, grazing, and mortality are a combination of elements from models presented by Banas (2011) and Ward et al. (2012) and discussed in more detail below. Trait (i.e., size) diffusion is formulated following Sauterey et al. (2017).

While we cast ecosystem dynamics in terms of size, many ecosystem models often include a representation of functional diversity (e.g. Moore et al., 2001; Quere et al., 2005), which groups species and

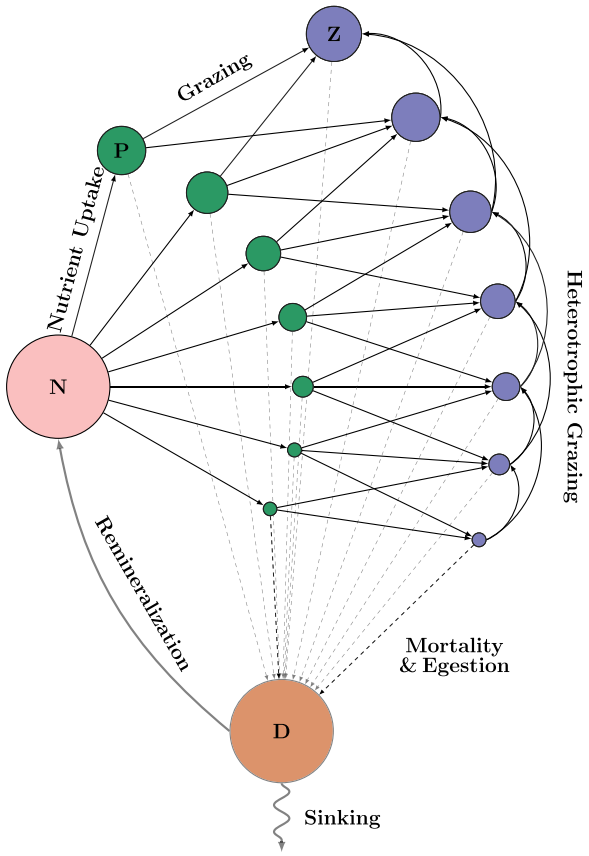

Fig. 1. Schematic of the size-structured ecosystem model used in this paper. Circles show individual model state variables (nutrient, phytoplankton, zooplankton and detritus biomass). Arrows show the direction of nutrient fluxes and interaction within the ecosystem, from a single nutrient pool to phytoplankton via uptake, from phytoplankton to zooplankton via grazing, and so on. This formulation allows for size-dependent preferential grazing in which zooplankton interact with several phytoplankton size classes, and, potentially, with other zooplankton.

taxa with similar nutrient uptake requirements or strategies to form a single functional group — e.g., cells that require silicon are modeled as the functional diatom group. Thus, each functional group provides a unique control on a biogeochemical pathway. While models based on functional groups have had success in predicting patterns of plankton distribution and productivity on a global scale (Gregg and Casey, 2007), they often require increased complexity relative to trait-based approaches (Follows and Dutkiewicz, 2011). Another challenge with this modeling approach is choosing the appropriate representation of functional groups to resolve the diversity in an ecosystem (Hood et al., 2006; Quere et al., 2005). Finally, functional groups are increasingly represented along a spectrum of different sizes (Ward et al., 2012; Dutkiewicz et al., 2020). Therefore, as a result of both reduced model parameter space and complexity, and a simplicity in representing ecosystem dynamics with allometric relationships, we focus on size alone as our primary axis of variability, with a single nutrient group and two size spectra of phytoplankton and zooplankton.

In the model, allometric relationships control phytoplankton nutrient uptake and limitation, zooplankton grazing rates, and size preference in predator–prey interactions (see Eqs. (6a)–(6b) and (10a)–(10b)). This formulation is informed by studies that show that smaller phytoplankton have faster nutrient assimilation rates and are less nutrient limited as a consequence of their small surface area to volume ratio (Eppley et al., 1969; Tang, 1995). On the other hand, large phytoplankton are more nutrient limited and have slower uptake rates. Additionally, smaller zooplankton have faster grazing rates compared to larger zooplankton (Hansen et al., 1994). We omit size dependence on zooplankton half-saturation rates in this model, however previous work by Edwards et al. (2012) has shown that half saturation rates with respect to size exhibit allometric behavior. This choice in our design is to minimize the number of allometrically defined variables and dependencies, as this other size structured ecosystem models include the same assumption.

Grazing dynamics is modeled after broad patterns of predator–prey size interactions. Here, we assume that small zooplankton graze prey of approximately the same size, while larger zooplankton prefer prey smaller than their own size (Hansen et al., 1994). While this is not the case for all zooplankton, and often depends on specific grazing strategies (Kiørboe, 2011), this functional form of grazing is commonly adopted in models (Moore et al., 2001; Poulin and Franks, 2010; Banas, 2011; Ward et al., 2012) with well documented grazing rates and preferential prey size (Hansen et al., 1994). Other representations of grazing includes the so-called "kill-the-winner" formulation, in which switching between optimal prey groups occurs, depending on prey abundance (Vallina et al., 2014). However, this formulation is dependent on many parameters that need be finely tuned. For the sake of simplicity, we model in this study a process referred to as "agnostic feeding" (Gentleman et al., 2003), which assumes that grazing pressures are constant between prey classes and, in this formulation, distributed only as a function of size.

Finally, while zooplankton and phytoplankton are separated into various sizes classes, detritus is collated as a single particulate group. While this simplification limits the use of the model to investigate the effect of plankton size structure on particle export and remineralization (Dunne et al., 2005; Richardson and Jackson, 2007), the detritus group could be easily expanded to incorporate variable size classes controlled by allometric relationships. However, uncertainty remains on the robustness of such relationships; for example, Iversen and Lampitt (2020) question the usefulness of particle size as an indicator of sinking speed, while other studies support it (Cael et al., 2021). Because the focus of this paper is plankton dynamics and size quantization, we opt to combine all detritus into a single sinking group (in 1D) for simplicity.

In the following, we outline each component of the model. Dependence on size is implicit, with the exception of size diffusion, and all functions in the model are written with respect to N, P, Z, and D. A schematic of the model is shown in Fig. 1; model parameters are summarized in Table 1.

2.2. Evolution equations

The following mass conservation equations express the time tendencies for a single nutrient akin to nitrate (N), phytoplankton (P), zooplankton (Z), and detritus (D), all expressed in units of nutrient (i.e., nitrogen) concentration (mmol m^{-3}). The number of phytoplankton size classes is n_p, and the number of zooplankton size classes is n_z. This model allows for an arbitrary number of zooplankton and phytoplankton sizes. The indexing variables for phytoplankton and zooplankton size classes are i and j respectively. Each evolution equation includes a component of physical forcing. In 0D, the physical forcing is a constant nutrient supply in the N equation. In 1D, nutrients are restored to an idealized profile, and all biogeochemical tracers are mixed by vertical diffusion.

The nutrient concentration N evolves in response to uptake by phytoplankton, remineralization, physical forcing:

$$\frac{\partial N}{\partial t} = \underbrace{\Gamma(N)}_{\text{Physical Forcing}} - \underbrace{\sum_{i}^{n_p} \mathcal{U}\left(N, P_i\right)}_{\text{Uptake by phytoplankton}} + \underbrace{\mathcal{R}(D).}_{\text{Remineralization}} \tag{1}$$

In 0D, physical nutrient supply takes a constant value (Section 3), while in 1D it is calculated via a restoring term (Section 2.8). In 1D, uptake of nutrients has additional functional dependencies on temperature and light.

The phytoplankton concentration evolves in response to nutrient uptake, grazing by zooplankton, linear mortality, and size diffusion:

$$\frac{\partial P_i}{\partial t} = \underbrace{\Gamma(P)}_{\text{Physical Forcing}} + \underbrace{\sum_i^{n_p} \mathcal{U}(N,P)}_{\text{Uptake by phytoplankton}} - \underbrace{\sum_j^{n_z} G\left(Z_j, P_i\right)}_{\text{Grazing by zooplankton}} - \underbrace{\mathcal{M}_p\left(P_i\right)}_{\text{Mortality}} + \underbrace{\varphi \frac{\partial^2}{\partial\left(\log_{10}\ell_i\right)^2} P_i}_{\text{Size diffusion}}, \tag{2}$$

where the length of the ith phytoplankton size is denoted as ℓ_i. Size diffusion in this model allows for small amounts of trait mutation and variability between phytoplankton and zooplankton along the size spectra (Sauterey et al., 2017), with the diffusion coefficient denoted as φ. Size diffusion is calculated in log-space, and described in Section 2.7. This addition to the SSEM captures the ability of plankton to adjust their size as a mechanism for niche selection (Merico et al., 2014).

The zooplankton concentration evolves in response to grazing of phytoplankton, heterotrophic grazing, a quadratic mortality term, and size diffusion:

$$\frac{\partial Z_j}{\partial t} = \underbrace{\Gamma(Z)}_{\text{Physical Forcing}} + \underbrace{\lambda \sum_i^{n_p} G\left(Z_j, P_i\right)}_{\text{Total uptake of phytoplankon}} - \underbrace{\sum_{j'}^{n_z} S\left(Z_{j'}, Z_j\right)}_{\text{Heterotrophic grazing loss}} + \underbrace{\lambda_s \sum_{j''}^{n_z} S\left(Z_j, Z_{j''}\right)}_{\text{Heterotrophic grazing uptake}} - \underbrace{\mathcal{M}_z\left(Z_j\right)}_{\text{Mortality}} + \underbrace{\varphi \frac{\partial^2}{\partial\left(\log_{10}\ell_j\right)^2} Z_j}_{\text{Size diffusion}}. \tag{3}$$

The size of the jth zooplankton size class is defined as ℓ_j. Both the grazing and self grazing profiles are presented as a functional dependence on the predator and prey, listed respectively in the function. For example, $G(Z,P)$ translates to the grazing of the predator zooplankton on the prey phytoplankton, and $S(Z_{j'}, Z_j)$ corresponds to the grazing of predator zooplankton, $Z_{j'}$ on the jth zooplankton size class, Z_j.

Finally the detrital concentration evolves in response to egestion or "messy grazing", phyto- and zooplankton mortality, remineralization, and sinking and removal:

$$\frac{\partial D}{\partial t} = \underbrace{\Gamma(D)}_{\text{Physical Forcing}} + \underbrace{(1-\lambda)\sum_i^{n_p}\sum_j^{n_z} G\left(Z_j, P_i\right)}_{\text{Egestion from grazing phytoplankton}} + \underbrace{(1-\lambda_s)\sum_j^{n_z}\sum_{j'}^{n_z} S\left(Z_{j'}, Z_j\right)}_{\text{Egestion from heterotrophic grazing}} + \underbrace{\sum_i^{n_p} \mathcal{M}_p\left(P_i\right)}_{\text{Phytoplankton mortality}} + \underbrace{\sum_j^{n_z} \mathcal{M}_z\left(Z_j\right)}_{\text{Zooplankton mortality}} - \underbrace{\mathcal{R}(D)}_{\text{Remineralization}} - \underbrace{\frac{\partial}{\partial z}\left(w_{\text{sink}} D\right)}_{\text{Particle sinking}}. \tag{4}$$

Note that the particle sinking term is calculated as an approximate sinking term in 0D and an explicit sinking term in 1D. The detritus equation serves to close the ecosystem model; in the absence of sources and sinks (nutrient forcing and removal via sinking), the size-structured NPZD model conserves total nutrient.

2.3. Nutrient uptake

Uptake is calculated using standard Michaelis–Menten dynamics that allows for a saturating response at high nutrient concentration (Franks, 2002), with additional functional dependence on local irradiance and temperature in 1D (Banas, 2011; Ward et al., 2012). This uptake is formulated as

$$\mathcal{U}(N,P_i) = U_i^{\max} \cdot \mathcal{I}(z,P) \cdot \mathcal{T}(z) \frac{N}{N + k_N^i} P_i, \tag{5}$$

where the light and temperature dependence functions are denoted as $\mathcal{I}(z,P)$ and $\mathcal{T}(z)$, respectively. In 0D both functions are set to constants, i.e., $\mathcal{I} = \mathcal{T} = 1$. In 1D, they are defined following Eqs. (26a) and (26b). The maximum uptake rate and half-saturation coefficient are allometric, following Banas (2011):

$$U_i^{\max} = a_u \left(\frac{\ell_i}{\ell_0}\right)^{b_u}, \tag{6a}$$

$$k_N^i = a_k \left(\frac{\ell_i}{\ell_0}\right)^{b_k}. \tag{6b}$$

All allometric parameters are given in Table 1. In this formulation, small phytoplankton benefit from fast uptake rates, and are less nutrient limited. Large phytoplankton, on the other hand, have slower rates of nutrient assimilation and are more nutrient limited (Tang, 1995; Banas, 2011; Ward et al., 2012).

2.4. Grazing

The grazing pressure is calculated as a function of predator and prey abundance, with an optimal predator–prey length scale, and a grazing preference represented by the width of a grazing profile. Banas (2011) and Ward et al. (2012) note that formulating the grazing profile in this way assumes that the encounter rate between predator and prey decreases outside of an optimal window, meaning that small prey are hard to detect by large predators. On the other hand, very large prey are less efficient forms of nutrient ingestion. This is commonly represented by a log-normal distribution, $\vartheta_{j,i}$, about an allometrically defined optimal predator–prey length scale, ℓ^{opt}, with a grazing profile width of $\Delta\ell$.

In this formulation, we assume that zooplankton heterotrophically graze on any plankton (phytoplankton or zooplankton) of a specific size with equal preference. Eqs. (7) and (8) model grazing as interactions between a predator zooplankton, Z_j, phytoplankton prey P_i and zooplankton prey $Z_{j'}$. Grazing is formulated using Michaelis–Menten dynamics (Franks, 2002; Banas, 2011; Ward et al., 2012) and depends on the total stock of prey plankton B_j, and half saturation coefficient k_p. Prey refuge is defined by Eqs. (12a)–(12b), which reduces grazing when the stock of prey becomes scarce.

The general form for grazing interactions between phytoplankton and zooplankton is

$$G(Z_j,P_i) = G_j^{\max} \frac{\vartheta_{j,i} P_i}{k_P + B_j} \cdot \mathcal{F}(P_i) \cdot Z_j, \tag{7}$$

where the jth zooplankton class grazes the ith phytoplankton size class. The component of heterotrophic grazing is defined as

$$S(Z_j,Z_{j'}) = G_j^{\max} \frac{\vartheta_{j,j'} Z_j}{k_P + B_j} \cdot \mathcal{F}(Z_{j'}) \cdot Z_j, \tag{8}$$

where the jth zooplankton class grazes the j'-th zooplankton size class. The total biomass available for grazing by the jth predator is defined as

$$B_j = \sum_i^{n_p} \vartheta_{j,i} P_i + \sum_{j'}^{n_z} \vartheta_{j,j'} Z_{j'}. \tag{9}$$

Following Banas (2011) and Ward et al. (2012), the maximum uptake rate of phytoplankton by zooplankton along with the optimal predator–prey length scale are allometrically defined by,

$$G_j^{\max} = a_g \left(\frac{\ell_j}{\ell_0}\right)^{b_g}, \tag{10a}$$

$$\ell_j^{\text{opt}} = a_l \left(\frac{\ell_j}{\ell_0}\right)^{b_l}. \tag{10b}$$

These relationships prescribe that small zooplankton graze prey more efficiently than large zooplankton (Hansen et al., 1994). Predator–prey size interactions also vary with respect to predator size: small

zooplankton tend to graze prey around the same body length as their own, whereas large zooplankton tend to graze prey that are much smaller than their own size (Hansen et al., 1994). In this formulation, the maximum zooplankton size is set by the largest size class present in the phytoplankton spectra.

The grazing preference of each zooplankton size class, on each prey size class is defined by a $n_p \times n_z$ matrix, represented by,

$$\vartheta_{j,i} = \exp\left[-\left(\frac{\log_{10}(\ell_i) - \log_{10}(\ell_j^{\text{opt}})}{\Delta\ell}\right)^2\right]. \tag{11}$$

The total amount of biomass available to each zooplankton size class is represented by the sum in the denominator in Eq. (7), with the total available biomass for each phytoplankton size class represented in the numerator. Finally, the functions $\mathcal{F}(P_i)$ and $\mathcal{F}(Z_j)$ limit the grazing pressure when the total phytoplankton and zooplankton prey biomass is small, respectively, i.e.,

$$\mathcal{F}(P_i) = 1 - \exp\left(-\sum_j \vartheta_{j,i} P_i\right), \tag{12a}$$

$$\mathcal{F}(Z_{j'}) = 1 - \exp\left(-\sum_j \vartheta_{j,j'} Z_{j'}\right). \tag{12b}$$

These zooplankton and phytoplankton prey refuge functions, $F(\bullet)$ are defined separately to simulate preference in grazing when one population of prey becomes particularly dominant (Mayzaud and Poulet, 1978).

2.5. Mortality

The mortality terms in the ecosystem are formulated linearly for phytoplankton and quadratically for zooplankton. Phytoplankton mortality is almost always modeled as a linear process in NPZD models and SSEMs (Franks, 2002; Poulin and Franks, 2010; Banas, 2011; Ward et al., 2012), whereas zooplankton mortality varies between models (Record et al., 2014). A quadratic mortality reflects the assumption that mortality processes not explicitly represented by the model, e.g. disease or grazing by predators outside the modeled size spectrum, are proportional to the total zooplankton stock, $\sum_j Z_j$. (Murray and Parslow, 1999) and Franks (2002) describe the response of a NPZ model with quadratic mortality and show that, at steady state, phytoplankton biomass increased until nutrient uptake or zooplankton grazing became saturated at the highest loads. By using a quadratic mortality in this model, we are able to simulate the effect of higher trophic level grazing on zooplankton, and allows for the nutrient uptake to become saturated in this model, which in turn allows for large phytoplankton size classes to be represented. The phytoplankton mortality is given by,

$$\mathcal{M}_p(P_i) = \mu_p U_i^{\max} P_i, \tag{13}$$

and

$$\mathcal{M}_z(Z_j) = \zeta Z_j \sum_{j'} Z_{j'}. \tag{14}$$

Here ζ is diagnosed by Banas (2011) to be,

$$\zeta = \frac{\overline{G_{\max}^2}\lambda}{4\overline{U_{\max}}\, k_p}. \tag{15}$$

where overbars denote averages over the uptake and grazing rates for all size classes of phytoplankton and zooplankton, respectively. To diagnose the value of ζ, we use a high resolution grid and calculate the uptake and grazing rates, finding that $\zeta = 1.7$ 1/(mmol N d), and fix this value for all runs in both the SSEM and the ROEM (Section 5).

2.6. Nutrient remineralization, forcing and sinking

Remineralization is formulated following (Dutkiewicz et al., 2009, 2012; Banas, 2011; Ward et al., 2012), as a linear function:

$$\mathcal{R}(D) = r_{\text{n}} D. \tag{16}$$

This represents bacterial processes by which particulate organic material is remineralized back into inorganic form.

Sinking of particles is the dominant process via which organic material is exported from the surface to depth (McCave, 1975). This serves to reduce near-surface remineralization and increase sub-surface nutrient concentration (Ducklow et al., 2001). In our model, we represent detritus as an aggregate group that sinks at a constant rate (Iversen and Lampitt, 2020). To simulate sinking particles in 0D, we assume a sinking speed, w_{sink}, and a mixed-layer depth, H_{sml}, and approximate the tendency due to sinking and removal as,

$$\frac{\partial}{\partial z}\left(w_{\text{sink}} D\right)\Big|_0 = -\frac{w_{\text{sink}}}{H_{\text{sml}}} D. \tag{17}$$

The physical forcing in 0D is constant, and set to

$$\Gamma(N) = 2 \text{ mmol N/m}^3/d. \tag{18}$$

In 1D, the physical terms ($\Gamma(\bullet)$) are a combination of nutrient restoring and diffusion. The one-dimensional extension is described in Section 2.8.

2.7. Size diffusion

Adaptations/mutations in the phytoplankton and zooplankton populations are represented as a trait diffusion process, based on the assumption that the phenotypic effect of mutations is small, random, and continuous in size space (Sauterey et al., 2017). Diffusion is calculated in log-size space so that diffusion is not skewed toward smaller sizes along the size spectra:

$$\varphi \frac{\partial^2}{\partial\left(\log_{10}\ell_i^2\right)} P_i = \varphi\left[\frac{1}{\Delta_{i-1/2}^2} P_{i-1} - \left(\frac{1}{\Delta_{i+1/2}\Delta_{i-1/2}} + \frac{1}{\Delta_{i-1/2}^2}\right) P_i + \frac{1}{\Delta_{i+1/2}\Delta_{i-1/2}} P_{i+1}\right], \tag{19a}$$

$$\Delta_{i-1/2} = \log_{10}(\ell_i) - \log_{10}(\ell_{i-1}), \tag{19b}$$

$$\Delta_{i+1/2} = \log_{10}(\ell_{i+1}) - \log_{10}(\ell_i). \tag{19c}$$

Here φ is given in Table 1, and ℓ_i is the size of the phytoplankton cell. The coefficient of diffusion is taken from Sauterey et al. (2017). Sauterey et al. (2017) determined that the total number of biomass peaks in the spectra is inversely correlated with the diffusion coefficient. In our model, we allow for weak size diffusion that supports the same number of species as solutions without size diffusion, while still allowing for weak trait evolution. The purpose of this choice is to limit the sharpness of the peaks and allow for small deviations about the optimal plankton size. Without size diffusion, biomass peaks are increasingly sharp, and their width is eventually determined by the numerical resolution in size space. The solutions at higher diffusivities given in Table 1 allow for wider peaks at steady state, but do not significantly affect the overall center of mass or total biomass.

2.8. Extension to 1D

We conduct most of the analysis in 0D (Section 3). However, in Section 4 we extend our analysis to 1D, to investigate the role of spatial heterogeneity. Here, we describe the model extension to 1D.

Table 1
Parameters and values of the size structured ecosystem model. All parameters without specific references are configuration-dependent and can change between experiments.

Parameter	Value	Units	Description	Reference
α	0.45		Percentage of light available for photosynthesis	Moore et al. (2001)
a_g	25	1/d	Coefficient of allometric grazing rate	Hansen et al. (1994)
a_k	0.1	μMN	Coefficient of allometric nutrient limitation	Eppley et al. (1969)
a_l	0.5	µm	Coefficient of optimal predator–prey length scale	Hansen et al. (1994)
a_u	2.6	1/d	Coefficient of allometric nutrient uptake	Tang (1995)
b_g	−0.4		Exponent of allometric grazing rate	Hansen et al. (1994)
b_k	1		Exponent of allometric nutrient limitation	Eppley et al. (1969)
b_l	0.65		Exponent of optimal predator–prey length scale	Hansen et al. (1994)
b_u	−0.45		Exponent of allometric nutrient uptake	Tang (1995)
H_{sml}	50	m	Mixed-layer depth	–
k_c	0.04	m	Absorption coefficient for photosynthesis	Moore et al. (2001)
k_w	0.03	m	Absorption coefficient for water	Moore et al. (2001)
φ	$[0, 3.7 \times 10^{-7})$	$\log 10(\mu\text{m})^2/\text{d}$	Size diffusion coefficient	Sauterey et al. (2017)
P^{init}	0.1	mmol N/m^3	Initial concentration of phytoplankton	–
Q_{sw}	340	W/m^2	Surface irradiance	Moore et al. (2001)
r	0.05		Temperature dependence	Ward et al. (2012)
r_{n}	0.04	1/d	Remineralization rate	Ward et al. (2012)
T_0	10	^{o}C	Reference temperature	–
μ_p	0.02		Phytoplankton mortality (fraction of growth rate)	Banas (2011)
w_{sink}	10	m/d	Detritus sinking speed	–
Z^{init}	0.01	mmol N/m^3	Initial concentration of zooplankton	–
ζ	1.7	1/(mmol N d)	Quadratic zooplankton mortality	

Table 2
Physical parameters used to run the size structured ecosystem model in 1D.

Parameter	Value	Units	Description
H_{exp}	150	m	Decay scale for surface temperature
H_{rd}	15	m	Minimum depth of non-zero restoring for nutrients
H_{sml}	25	m	Imposed depth of mixed layer
κ_{bg}	10^{-4}	m^2/s	Background vertical diffusivity
κ^0_{sml}	10^{-1}	m^2/s	Maximum surface mixed layer vertical diffusivity
N_{max}	25	mmol N/m^3	Maximum nutrient concentration at depth
N_H	80	m	Decay scale for nutrients
T_0	10	° C	Reference temperature for nutrient uptake
T_{max}	22	° C	Maximum temperature at the surface
T_{max}	4	° C	Minimum temperature in the water column

2.8.1. Restoring and diffusion

Vertical dynamics have a first order impact on the distribution of phtyoplankton within the euphotic zone as a consequence of mixing within the surface mixed layer and light- and temperature-limitation (Ryabov et al., 2010; Klausmeier and Litchman, 2001; Beckmann and Hense, 2007; Venrick, 1993). Within the surface layer, phytoplankton are vertically mixed and exposed to a variety of light conditions as a consequence of light attenuation (Sverdrup, 1953; Huisman et al., 1999; Obata et al., 1996; Mahadevan et al., 2012). If the mixed layer is sufficiently shallow, high concentration of chlorophyll are found in deep chlorophyll maxima as a result of the balance between light limitation and nutrient availability (Partensky et al., 1999; Cullen, 1982). Thus, in the presence of spatial variations in light and nutrient variability, these "bottom-up" influences on the ecosystem may be expected to affect the vertical distribution of different phytoplankton size classes.

Our 1-D model is an idealized, z-coordinate model with vertical mixing and nutrient-restoring in lieu of vertical advection. The timescale of restoring and profile of nutrients are tuned to approximate values chosen in the nutrient forcing experiments conducted in Section 3.3. The vertical diffusivity in the surface mixed layer is prescribed to have the same structure as used in the κ-profile parameterization (KPP) of Large et al. (1994). However, we simplify the formulation by fixing the mixed layer depth, H_{sml} and maximum magnitude, κ_{sml}, rather than computing these quantities from the surface forcing. Given a background diffusivity of $\kappa_{\text{bg}}(z)$, the vertical profile of the vertical mixing coefficient is

$$\kappa_{\text{dia}}(z) = \kappa_{\text{sml}}(z) + \kappa_{\text{bg}}(z). \tag{20}$$

Note that we do not include a bottom boundary layer in this formulation, under the assumption that the euphotic zone is shallower than the depth of the water column above the bottom boundary layer. The profile of κ_{dia} in the surface mixed layer, ie. $-H_{\text{sml}} < z < 0$, is given by,

$$\kappa_{\text{sml}}(z) = \kappa^0_{\text{sml}} G_{\text{KPP}}\left(\sigma_{\text{sml}}\right), \tag{21}$$

where the dimensionless surface mixed layer coordinate, $\sigma_{\text{sml}} = -z/H_{\text{sml}}$, is defined such that $\sigma_{\text{sml}} \in [0, 1]$ within the mixed layer, and all parameters are given in Table 2. The structure function is given by,

$$G_{\text{KPP}}(\sigma) = \begin{cases} \dfrac{27}{4}\sigma_{\text{sml}}(1-\sigma_{\text{sml}})^2, & 0 \le \sigma_{\text{sml}} \le 1, \\ 0, & \sigma_{\text{sml}} \ge 1. \end{cases} \tag{22}$$

The scaling factor of 27/4 ensures that the structure function has a maximum factor of 1 over the mixed layer. The tendency due to diffusion is calculated using an implicit diffusion scheme.

The nutrient forcing in the physical model is the restoring of nutrients to an idealized profile, in lieu of advection, and vertical mixing, which allows us to resolve a surface mixed layer. The profile of restoring is given by,

$$N_{\text{R}}(z) = N_{\text{surf}} - (N_{\text{max}} - N_{\text{surf}}) \tanh\left(\frac{z + H_{\text{rd}}}{N_H}\right), \tag{23}$$

where N_{surf} is the surface nitrate concentration, N_{max} is the maximum nitrate concentration at depth, N_H is the thickness of the nutricline, and H_{rd} is the depth at which the nutrient concentration begins to monotonically increase.

All runs are initialized using the same initial conditions, noting that the "init" subscript refers only to the initial profile:

$$N_{\text{init}}(z) = N_{\text{R}}(z), \tag{24a}$$

$$P_{\text{init}}(\ell_{i_p}, z) = P^{\text{init}}, \tag{24b}$$

$$Z_{\text{init}}(\ell_{i_z}, z) = Z^{\text{init}}, \tag{24c}$$

$$D_{\text{init}}(z) = 0. \tag{24d}$$

Here $N_{\text{R}}(z)$ is defined in Eq. (23), and the profiles of P, and Z are set to constant values P^0 and Z^0 for all sizes and depths, respectively (Table 1).

2.8.2. Temperature and light dependence

In a 1D framework, we additionally include dependence of nutrient uptake on temperature and light (see Eq. (5)). We use an idealized profile of coastal temperature motivated by measurements from California Cooperative Oceanic Fisheries Investigations (McClatchie, 2016), formulated following (Moscoso et al., 2021),

$$T(z) = T_{\min} + (T_{\max} - T_{\min}) \exp\left(\frac{z}{H_{\exp}}\right), \tag{25}$$

where all parameters are given in Table 2.

The profile of irradiance is calculated via the Beer–Lambert Law with coefficients following Moore et al. (2001). The profile of photosynthetically available light is integrated vertically at each time step to calculate the light attenuation by phytoplankton and zooplankton,

$$\frac{\partial I(z)}{\partial z} = -k_{\text{par}} I(z), \quad \text{where} \quad I_0 = I(z=0) = \alpha Q_{sw}, \tag{26a}$$

$$k_{\text{par}} = k_w + k_c \left(\sum_i P_i + \sum_j Z_j \right). \tag{26b}$$

The light-dependent uptake function represents a saturating response at high levels of irradiation (Franks, 2002):

$$\mathcal{I}(z, P) = \frac{I(z)}{\sqrt{I_0^2 + I(z)^2}}, \tag{27}$$

and the temperature component of the uptake function is formulated using a typical exponential equation (Franks, 2002; Ward et al., 2012),

$$\mathcal{A}(z) = e^{-r(T_0 - T(z))}. \tag{28}$$

with respect to a reference temperature T_0.

3. Emergent quantization

In this section, we characterize top-down and bottom-up controls on quantization in SSEMs using a set of experiments that independently control nutrient forcing and grazing with a finely-resolved size grid. Other SSEMs models have shown quantized behavior around a few intermediate size classes when a predator–prey grazing width is present (Banas, 2011; Sauterey et al., 2017) in 0D. However, what controls the location and robustness of the peaks in biomass is not well understood. Here, we perform experiments varying the size-space resolution, the nutrient forcing, and the width of the predator–prey interaction window.

We integrate the model under constant forcing for 100 years, which is longer than typical timescales of nutrient supply variability that are found in nature (Whitney et al., 1998; Messié et al., 2009). In all experiments, except those presented in Section 3.2, we resolve 200 phytoplankton and zooplankton size classes. For simplicity, we focus on the steady-state behavior achieved at very long timescales, and discuss the potential consequences of temporal variations in nutrient supply in Section 6. For example, we see that abrupt changes in the size structure, such as bifurcations, may even occur after several decades at constant forcing (see Fig. 2).

3.1. Evolution to quantization in a reference experiment

All experiments run in this study use a relatively weak, constant nutrient forcing, with a long timescale that allows for the internal dynamics of the ecosystem to evolve without additional perturbations. While steady state solutions can help inform ecosystem behavior, plankton are often impacted by ocean circulation on a variety of timescales from hours to months and longer (Deser and Timlin, 1997; Rodriguez et al., 2001; Lévy et al., 2001; Lévy, 2003). Therefore, understanding the spin-up behavior of our model from constant conditions can help understand solutions in more realistic physical setting.

We show an example of a time series during model spin-up in Fig. 2. Quantization in this and other model solutions occurs after a relatively short time scale ($\mathcal{O}$(days)) for the smallest phytoplankton and zooplankton, likely as a result of fast uptake rates and rapid grazing, which quickly balance bottom-up and top-down controls. Large phytoplankton on the other hand, have slower grazing rates, but weaker grazing pressures. This likely controls the location of the peaks (see Section 3.4) by optimizing predator–prey interactions and competition. We explore this behavior in more detail in Section 3.4. Quantization in phytoplankton biomass occurs on longer timescales than quantization in zooplankton biomass. This is likely a consequence of competitive exclusion, where large amplitude variations promote rapid exclusion of some zooplankton size classes (Barton et al., 2010). We note the presence of internal ecosystem variability in phytoplankton over the first 18 months, which forces small oscillations around the stable zooplankton size classes, while the phytoplankton spectra reaches stability. During this interval of time, the biomass peaks sharpen. In the longer-term, we see sharpening of biomass peaks to aggregate around a few specific size classes, a process that occurs over decades.

3.2. Sensitivity to resolution in size-space

Previous studies have found that ecological models with coarse resolution do not adequately capture phytoplankton diversity or quantization (eg. Ward et al. (2012) and Henson et al. (2021)), whereas models with a finely-resolved trait grid are able to capture diversity (eg. Banas (2011)). The purpose of this experiment is to demonstrate the number of size classes required both to achieve quantization in biomass, and ensure that the ecosystem solution is well resolved and accurate in the total concentrations of phytoplankton and zooplankton. We quantify the sensitivity to resolution by running a parameter sweep between resolving 5 and 200 size classes. A motivation for this experiment is to ensure that our model fully resolves steady state behavior and reaches convergence with respect to size-grid resolution. For all experiments, the minimum and maximum size of the phytoplankton are fixed, and the total biomass with respect to the resolution is shown in Fig. 3. Note that in the model, it is not necessary for the number of size classes to be the same between phytoplankton and zooplankton, but we opt for this configuration for simplicity. For our analysis, we calculate the concentration-weighted average size for the kth peak as

$$\ell_k^{\text{peak}} = \frac{1}{P_k^{\text{tot}}} \sum_{i=i_{\min,k}}^{i_{\max,k}} P_i \ell_i, \tag{29a}$$

$$P_k^{\text{tot}} = \sum_{i=i_{\min,k}}^{i_{\max,k}} P_i. \tag{29b}$$

Here the boundaries (in size space) for integration over the kth peak, defined by the indices $i_{\min,k}$ and $i_{\max,k}$, are defined by the locations of local biomass minima along the size spectrum. The locations of the zooplankton peaks in size space are defined analogously to Eqs. (29a)–(29b).

At the coarsest resolution, $n_p = n_z = 5$, the biomass along the phytoplankton and zooplankton size spectra is not quantized. As the resolution in size-space increases, quantization emerges. Phytoplankton and zooplankton biomass exhibits quantized behavior at 10 size classes, but these solutions are not fully resolved. Here, we consider solutions to be fully resolved when the biomass in each peak becomes insensitive to further refinements of the size grid. In this case, we assume convergence when variations in the total biomass between peaks varies by less than 5 percent with increasing resolution. By this metric, quantization in phytoplankton biomass is fully resolved with approximately 85 size classes, whereas quantization in zooplankton occurs at 130 size classes. However, this may be slightly conservative. Despite some oscillations in the zooplankton size classes, the behavior is nearly stabilized at 50 size classes. Regardless, we use a high resolution for the remainder of

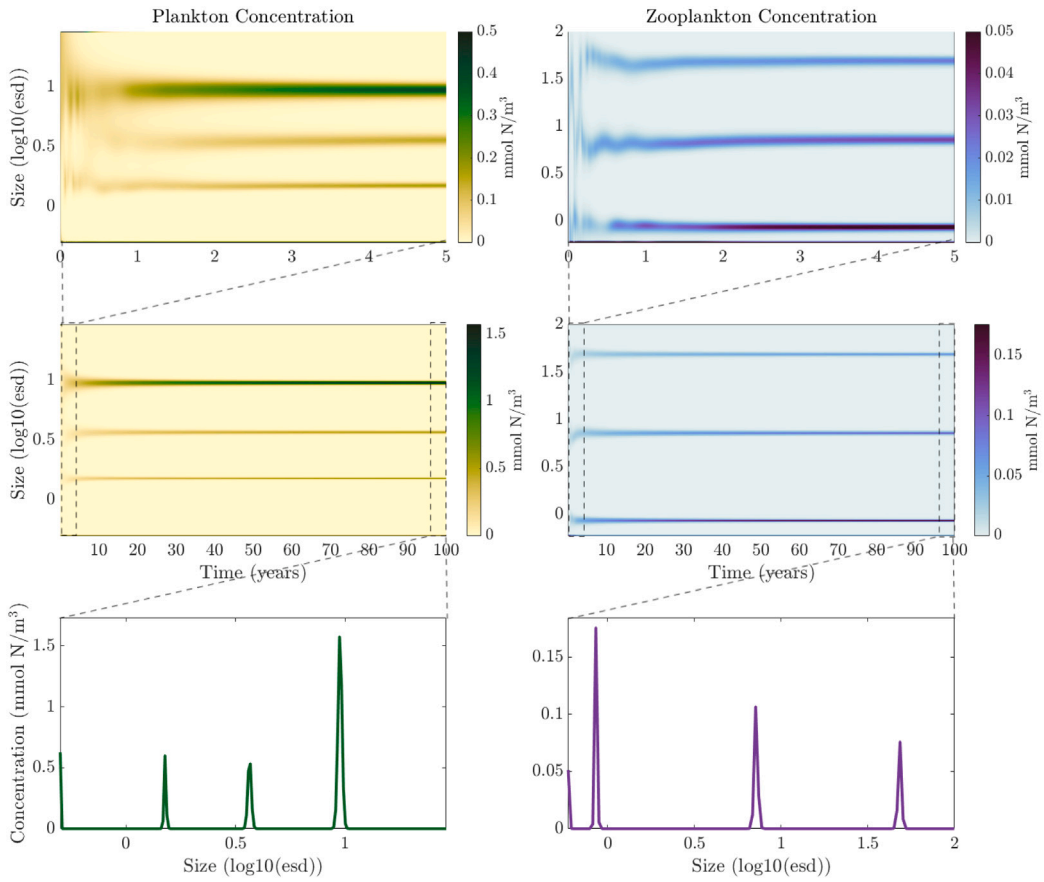

Fig. 2. Evolution of a reference experiment over one hundred years of integration. The left column shows the phytoplankton concentration, and the right column shows the zooplankton. The top row of this figure shows the plankton concentrations over the first five model years. Note that the colorbar has been shifted to show the internal ecosystem oscillations before becoming stable. The middle row shows the concentrations over the entire model run, and the bottom row shows the plankton concentration as a function of size, averaged over the final five model years.

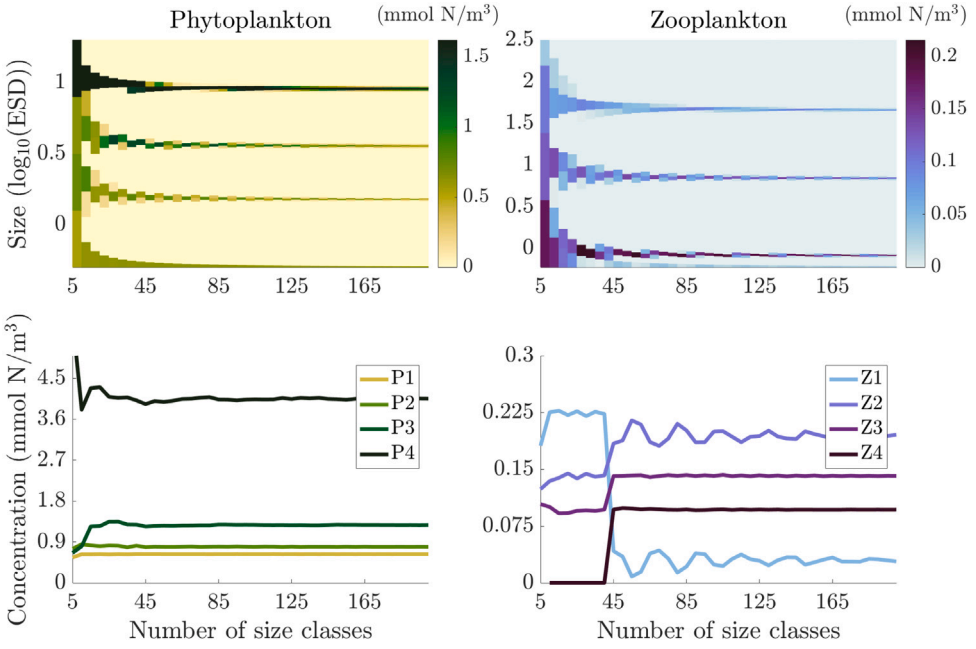

Fig. 3. Quantization with increasing resolution in size space. The top row shows the parameter sweep diagram, the bottom row shows peak-integrated concentrations. Left column shows phytoplankton biomass, right column shows zooplankton biomass. *P*1 indicates the smallest non-zero biomass peak, *P*2 indicates the second smallest non-zero biomass peak, and so on. The same numbering convention is used for the zooplankton biomass peaks.

the sensitivity experiments — 200 phytoplankton and zooplankton size classes to ensure that solutions are fully resolved.

Model changes with finer grid size indicate that zooplankton are more sensitive than phytoplankton to size resolution. With 10 size classes, the maximum number of biomass peaks (4) for this configuration emerges. The total biomass in each peak is approximately the same, with the largest size class contributing to most of the phytoplankton biomass. Zooplankton biomass, however, changes substantially as a function of grid resolution after the emergence of quantization. Specifically, at low resolution, the smallest size class has the highest concentration of biomass, whereas at high resolution, the second size class has the highest concentration of biomass. An explanation for this is that grazing favors intermediate zooplankton size classes, because the smallest zooplankton experiences the most predation pressure.

3.3. Sensitivity of quantization to external forcing

Nutrient supply ultimately determines the total biomass and dominant size of phytoplankton in both models and observations (Worden et al., 2004; McQueen et al., 1986; Chenillat et al., 2013; Verity and Smetacek, 1996; Chavez, 1989; Armstrong, 1994). At high nutrient concentrations, a large fraction of the phytoplankton biomass is concentrated within intermediate and large phytoplankton (Chisholm, 1992; Cavender-Bares et al., 2001; Venrick, 2002). At low nutrient concentrations, most of the phytoplankton biomass is concentrated within small size classes. We conduct two sets of experiments to investigate the response of the model to different nutrient forcing strengths. The first set shows responses to direct changes in nutrient supply rate. The second set restores phytoplankton and zooplankton to a constant small concentration at two different timescales to examine the robustness of quantization in the presence of external sources and sinks. This experiment is designed to mimic reduction of total biomass over different timescales, and may be conceptualized as representing horizontal variability or dilution.

Fig. 4 shows the ecosystem response to a variation in nutrient forcing spanning the range between 0.1 and 3 mmol N/m^3/d. The higher end of this nutrient forcing is likely unrealistically large over the long timescales of the experiments. However, Hales et al. (2005) found similarly large nutrient supply averaged over the depth of the mixed layer during an upwelling event. The lower end of this parameter space represents oligotrophic waters (Johnson et al., 2010). At the lowest levels of nutrient forcing ($F \leq 0.1$ mmol N/m^3/d) there is only one biomass peak, consistent with typical oligotrophic, open-ocean conditions (Partensky et al., 1999). At the highest nutrient forcing, the intermediate and large biomass peaks increase in overall biomass, and the largest biomass peak drifts toward larger sizes.

Zooplankton respond indirectly to variations in nutrient forcing, via its impact on the phytoplankton biomass, and similarly exhibit bifurcations in the biomass peaks as the nutrient forcing is increased. At high nutrient forcing, there is an additional bifurcation in the zooplankton distribution at an intermediate size class. This is likely a result of the biomass loading of the largest and second largest phytoplankton size classes, which allows for another large zooplankton class to persist. Additionally, the largest size peak in zooplankton increases along to optimize the spacing between other zooplankton classes and grazing on the largest phytoplankton peak.

A robust feature of this experiment is that the approximate location of the phytoplankton peaks, and, to some extent, the zooplankton peaks as well, is nearly constant away from bifurcation points. This indicates that while the bottom-up control determines the overall abundance of phytoplankton and the dominant size class (Partensky et al., 1999; Worden et al., 2004; Venrick, 1982; Armstrong, 1994), the top-down control may be more important in determining the locations of the biomass peaks along the size spectra (Cavender-Bares et al., 2001; Chisholm, 1992; Venrick, 2002). We explore this behavior in Section 3.4.

We next examine the robustness of quantization by performing experiments in which we restore the phytoplankton and zooplankton concentrations to small values. We restore using three different timescales: 6 months, 1 year, and 5 years. These timescales are representative of different behavior during spin-up (see Fig. 2).

We set the restoring to be $P_{\text{restoring}} = P^{\text{init}}$ so that all size classes are restored toward a profile without size-quantization in biomass, see Figure Fig. 5. We similarly force the zooplankton concentration to the initial concentration Z_{init} using the same restoring timescales. The restoring is calculated as an linear damping with respect to the restoring timescale T_r (see Fig. 5).

At the fastest restoring timescale, there is still some residual quantization, similar to the dynamics that occur in early spin-up times. At fast restoring timescales, the smallest size class is the most robust as a consequence of fast uptake rates (Tang, 1995; Partensky et al., 1999). On longer restoring timescales, the largest phytoplankton size classes contain a substantial fraction of the phytoplankton biomass. This implies that while quantization and the approximate center of mass for each peak is established at shorter timescales, sharpening of the peaks occurs on very long timescales.

The zooplankton exhibits a similar response to the imposed restoring. However, the largest size classes in both the fast and slow restoring experiments are significantly broader than in the steady state solution with no restoring. Because the biomass in the fast restoring case is located over a wider range of size classes, the largest zooplankton size class can graze a broader range of sizes with less phytoplankton limitation. Thus, with these experiments, we conclude that the concentration-weighted size of the largest phytoplankton mode – and thus zooplankton via grazing – is dependent on the bottom-up nutrient forcing (see Fig. 4). To better understand what controls the location of the quantized solutions, we test various grazing profiles and prey-selectivities.

3.4. Grazing profile width

Here, we vary the predator–prey selectivity window $\Delta\ell$ in Eq. (11) to understand the behavior of the ecosystem with narrowed and broadened selectivity, *i.e.* with smaller $\Delta\ell$ and larger $\Delta\ell$ respectively. With increased grazing selectivity, the size window in predator–prey interactions decreases, limiting the overall amount of total phytoplankton available to a single zooplankton class. With reduced selectivity, a single zooplankton size class is able to graze a wider variety of phytoplankton sizes. Fig. 6 shows a bifurcation diagram varying the predator–prey interaction window. We define the distance between biomass peaks as the distance (in size space) between the concentrated-weighted sizes, *i.e.* the difference, $l_{k+1}^{\text{peak}} - l_k^{\text{peak}}$, between adjacent biomass peaks.

Bifurcations in size space reflects trade-offs between bottom-up nutrient availability and top-down grazing pressures, by which phytoplankton optimize their total biomass with respect to size — a driver for quantization. For example, small phytoplankton are less nutrient limited, but have the highest grazing pressure (Tang, 1995). A trade-off in this case would tend to shift biomass toward faster uptake rates and less nutrient limitation over the heavy grazing pressure. Alternatively, large phytoplankton are more nutrient limited but have less overall grazing pressure. A trade-off for large phytoplankton is to tend toward reduced grazing pressure under higher resource competition (Hansen et al., 1994).

With broader prey-selectivity windows, there are fewer biomass peaks along the phytoplankton and zooplankton size spectrum. As the grazing window shrinks, and zooplankton become more selective, a series of pitchfork bifurcations occur, which give rise to more biomass peaks along the size spectrum, filling niches generated by reduced grazing pressure (Loeuille and Loreau, 2005). At smaller grazing profile widths, more biomass peaks are found along the size spectrum, and in the limit where $\Delta\ell \to 0$, the biomass is no longer quantized. We found

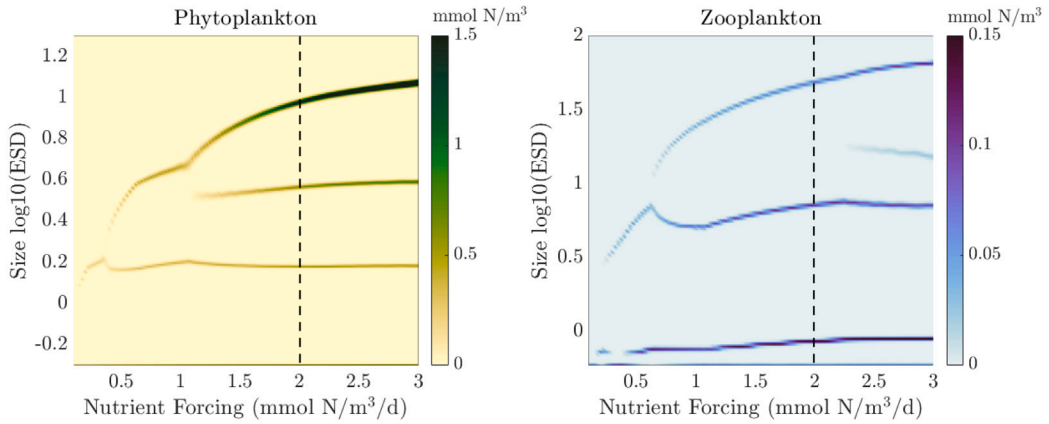

Fig. 4. Bifurcation diagram for different nutrient forcing. The dashed line shows the location of the value used as a reference nutrient forcing for other experiments.

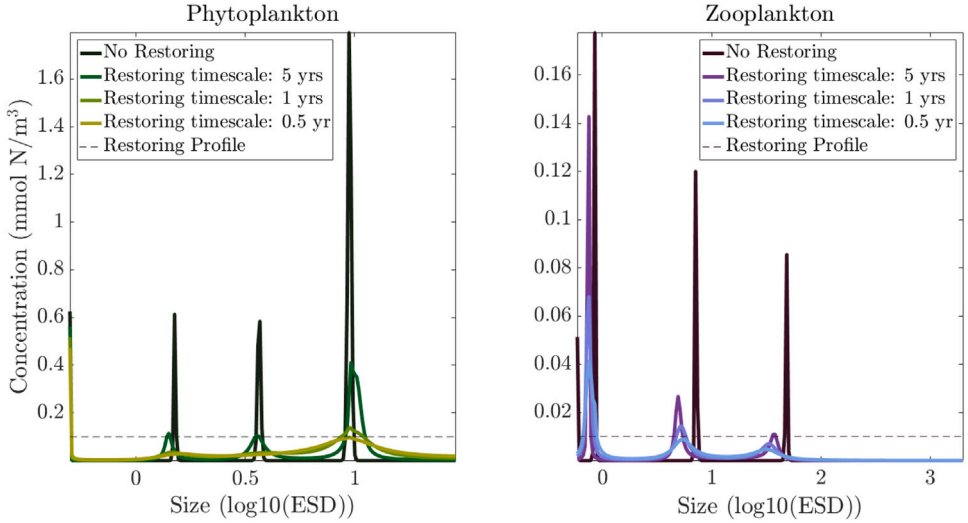

Fig. 5. Phytoplankton and zooplankton quantization in solutions with restoring to a small constant concentration (black dotted line) over time scales of 5 years, 1 year, and 0.5 years.

that there still exits quantization at very small values of $\Delta\ell \sim 0.01$, assuming that the size grid is adequately resolved.

The distance between biomass peaks has an approximately linear relationship with the grazing window when plot in log–log space (Fig. 6, bottom), i.e. the relationship can be approximated by a power-law. However, as a consequence of bifurcations, the linear relationship is less accurate near bifurcation points.

In these experiments the phytoplankton biomass peak with the largest organism size is strongly sensitive to the grazing window width. The zooplankton biomass peak with the largest concentration-weighted size, however, has nearly the same size at all grazing profile widths, varying non-monotonically by a multiple of approximately 1.8 over the range of grazing windows considered here. We can explain this behavior as result of trade-offs between grazing pressure, nutrient limitation, and uptake rates (McQueen et al., 1986). On one hand, more biomass peaks along the size spectrum are able to coexist with a narrower grazing window. On the other hand, with increased phytoplankton biomass peaks there is more resource competition between various size classes, benefiting smaller phytoplankton cells and reducing the size of the largest phytoplankton.

To better understand the relationship between the grazing profile width and the locations (in size space) of the biomass peaks, we consider the grazing pressure of zooplankton on phytoplankton in our reference experiments ($\Delta\ell = 0.1, 0.2, 0.3$). We define a peak-integrated grazing pressure, $G^{\text{tot}}_{i,k}$ as the phytoplankton-biomass normalized grazing rate for each integrated zooplankton size class, Z^{tot}_k, e.g.

$$G^{\text{tot}}_{i,k} = \frac{1}{P_i} \sum_{j=j_{\min,k}}^{j=j_{\max,k}} G(Z_j, P_i). \tag{30}$$

This metric quantifies the total rate of grazing of the ith phytoplankton due to the kth zooplankton biomass peak. Without the normalization to a rate (*i.e.* units of s^{-1}), this metric would be dominated by the locations of the phytoplankton biomass peaks.

In Fig. 7 we plot the total grazing pressure along the phytoplankton size spectrum. The maxima in grazing pressure do not coincide with peaks in phytoplankton biomass; rather, the phytoplankton biomass peaks fall instead in the "shadow zones" of the grazing profile, emerging as a balance between grazing pressure and uptake rates, which dynamically co-vary. Due to the non-linearity and large number of phytoplankton and zooplankton size classes, predicting the exact location of the biomass peaks with the full system is challenging. However, Fig. 7 lends insight into the relationship between grazing profile width and the spacing between biomass peaks (Fig. 6): widening the grazing profile widens the space between"shadow zones" in which the phytoplankton biomass peaks fall.

We note that zooplankton self-grazing (not shown) does not have as much as an effect on the location of the biomass peaks in the zooplankton size spectra. Instead, it redistributes the total biomass from small zooplankton to large phytoplankton, as the self-grazing strength increases.

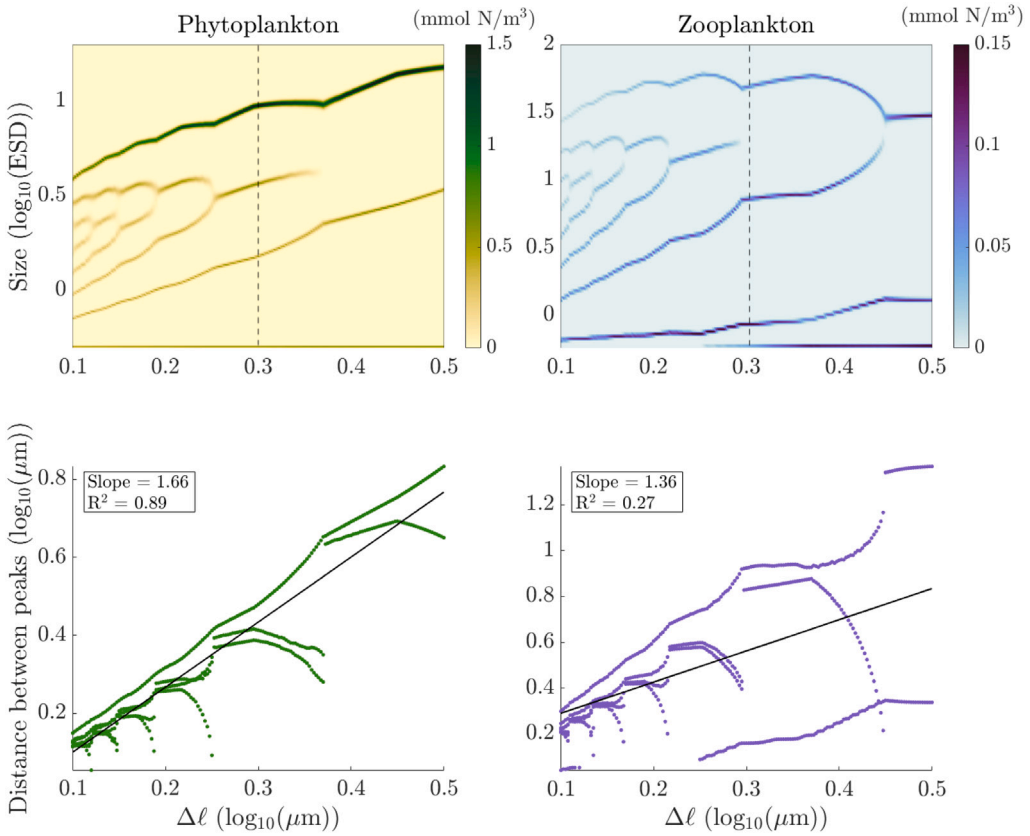

Fig. 6. This figure shows bifurcation diagrams with respect to the grazing profile width $\Delta\ell$ (top) and distance between the center of mass of each biomass peak (bottom), with respect to phytoplankton biomass (left) and zooplankton biomass (right).

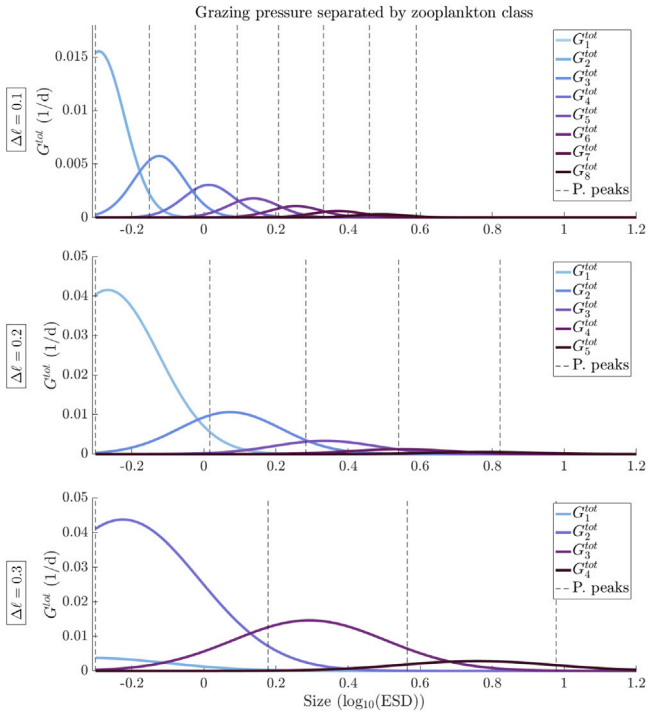

Fig. 7. Normalized grazing rate of each phytoplankton size class due to each zooplankton biomass peak. The vertical dashed lines indicate the sizes of the phytoplankton biomass peaks.

4. Persistent quantization in 1D

We now use our 1D model setup (Section 2.8) to examine quantization in a vertically heterogeneous environment that, while idealized, provides a first order representation of environmental gradients found in the ocean. The solutions shown in Fig. 8 are forced with three different nutrient supply strengths, N_{surf} = 0 (top row), 1 (center row), and 2 mmol N/m^3/d (bottom row), corresponding respectively to oligotrophic, intermediate, and eutrophic conditions.

In the 1D framework, quantization persists in the presence of vertical diffusion, variable nutrient supply, and variable light- and temperature-limitation (Fig. 8). As a result of low nutrient concentration, the smallest phytoplankton class contains all of the biomass at the surface, whereas at depth, larger phytoplankton contribute to the high biomass concentration. Zooplankton solutions (not shown) are similarly quantized. At depth, the largest phytoplankton outcompete smaller phytoplankton. At high nutrient forcing throughout the mixed layer, intermediate and large phytoplankton are responsible for most of the biomass and outcompete smaller phytoplankton at depth. We note that between the two solutions in 0D and 1D, the phytoplankton biomass is approximately distributed in the same size classes.

Surprisingly, we find no vertical variations of phytoplankton size even with vertical variations in nutrient supply (see Fig. 4). This suggest that a vertically heterogeneous environment is still able to support homogeneous quantization. A possible explanation is the presence of vertical mixing of the dominant size classes, which in turn out-compete other groups. This finding is consistent with 0D studies (Banas, 2011) that show that size quantization is robust to seasonal variations in nutrient supply.

We now repeat the experiments discussed shown in Section 3.4, varying the grazing selectivity window $\Delta\ell$ in the 1D framework. Once

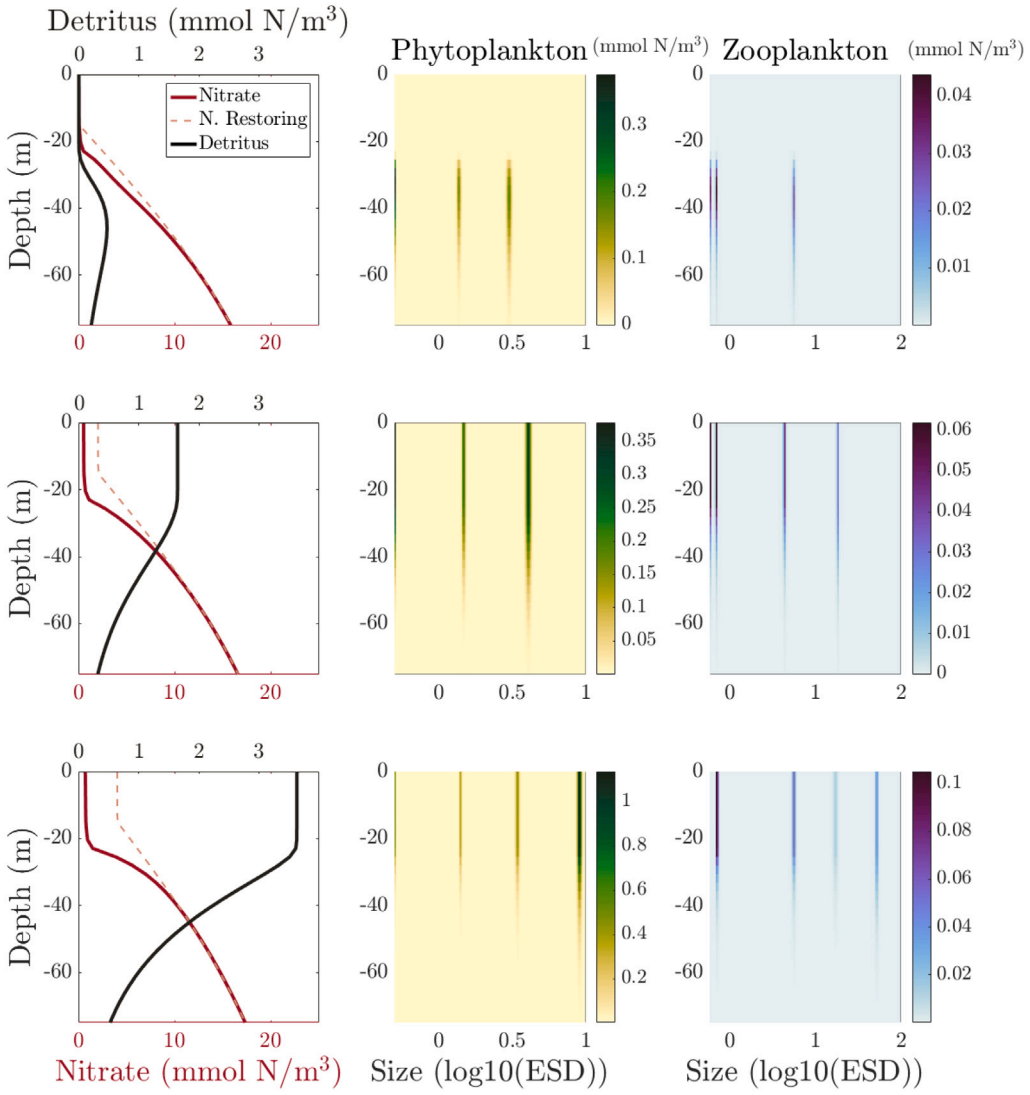

Fig. 8. The final profiles for nitrate, phytoplankton, zooplankton, and detritus with respect to depth in the 1D model with surface mixed layer estoring rates of 0 mmol N/m^3/d (top), 1 mmol N/m^3/d (center), and 2 mmol N/m^3/d (bottom) to show the response under various surface nutrient forcing. Concentrations of organic and inorganic nitrate (left), phytoplankton (center), and zooplankton (right) are shown.

each solution has reached steady state, we integrate the biomass vertically through the water column and then compute the concentrated-weighted, vertically-integrated biomass peak locations in size space using Eqs. (29a)–(29b). Since the size of the largest phytoplankton peak is dependent on the total nutrient forcing (Section 3.3), we use the largest surface nutrient forcing (see bottom row in Fig. 8) to ensure that the largest phytoplankton size class is represented.

We find qualitatively similar behavior between the 0D and 1D parameter sweeps, with a series of pitchfork bifurcations in the plankton biomass as the width of the grazing profile decreases. Due to the similarities, we do not include an additional bifurcation diagram. The spacing between peaks retains a nearly linear relationship away from regions containing bifurcations (see Fig. 6). We additionally find a strong correlation between the size of the largest phytoplankton mode and the grazing profile width in 1D. There are some minute differences between the bifurcation diagram in 0D and 1D, for example in the exact locations of the bifurcation points in Δl space. We suspect that this may be caused by vertical light- and temperature-limitation terms, and not by any internal ecosystem dynamics.

5. Reduced order ecosystem modeling

The SSEM experiments show that quantization is a robust feature in size structured ecosystem models even in a variable environment, and that the width of the grazing profile determines the location of biomass peaks along the spectrum in both 0D and 1D. This robustness of quantization motivates us to reduce the complexity of the SSEM, approximating each of the biomass peaks as a single size class along the size spectrum. The purpose of this approach is to help inform methods of discretization in models that are not able to resolve a large number of size classes. Often models that fix the size of phytoplankton to general sizes (eg. pico-, nano-, and microplankton) may miss the inherent quantization and thus diversity in the solutions for the ecosystem (Henson et al., 2021). We refer to the model we propose as a Reduced-Order Ecosystem Model (ROEM).

5.1. Model reduction in size space

The ROEM takes advantage of robust quantization and reduces the entire size spectrum to a few representative points along the biomass spectrum. However, because the correlations between the peak distance

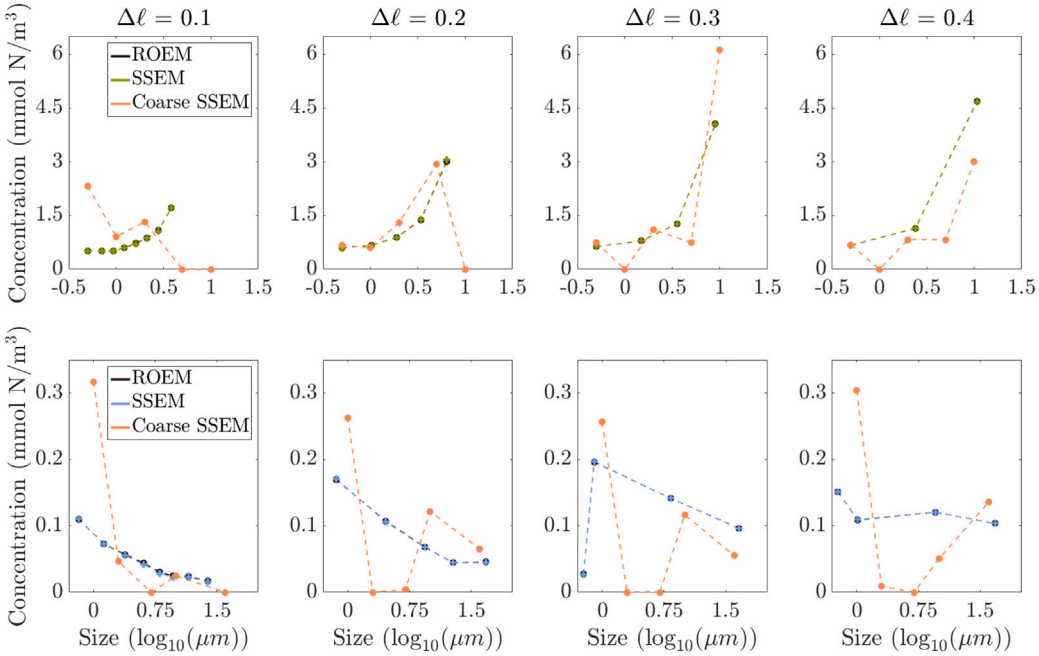

Fig. 9. Comparison with the biomass in 0D solutions of the reduced order ecosystem model, compared with the total biomass in each corresponding peak from SSEM. The top row shows the phytoplankton solutions from the ROEM (black), high resolution SSEM (green), and coarse SSEM (orange). The bottom row shows zooplankton solutions from the ROEM (black) and SSEM (purple), and coarse SSEM (orange).

and grazing profile width deviate from a linear relationship near bifurcation points, we are unable to find an a priori relationship that accurately predicts the location of the peaks for arbitrary values of the predator–prey selectivity window, $\Delta\ell$. Instead, this process is done numerically from a 0D solution for a specific grazing profile width. Because the model behavior is approximately the same between 0D and 1D, the location of the biomass peaks in 0D should be sufficient to predict the location of the peaks in 1D, even with some degree of heterogeneity in nutrients, temperature, or light. While the ROEM is derived from a steady state solution of the SSEM in 0D, a reduced order model can increase computational efficiency in higher spatial dimensions, while still providing a representation of ecosystem behavior consistent with the SSEM.

In order to obtain each representative size class, we make the assumption that modes along the biomass spectrum can be represented as a delta function along the size spectra. We select the locations of the phytoplankon and zooplankton size classes in by calculating the concentration-weighted average sizes of each biomass peak (see Eq. (29a)). For all solutions shown in Fig. 2, the number of size classes used in the ROEM are equal to the number of biomass peaks. Furthermore, the size classes used are specifically ℓ_k^{peak}. We test the performance of the ROEM in 0D and 1D, see Figs. 9 and 10.

5.2. Model testing

Fig. 9 shows a comparison of the SSEM and the ROEM in 0D. We compare the biomass between a finely discretized SSEM ($n_p = 200$), a coarsely discretized SSEM ($n_p = 5$), and the corresponding representation with the ROEM. Each point corresponds to the integrated biomass in each peak using Eq. (29b). The ROEM captures the phytoplankton and zooplankton biomass well over various grazing profile widths. However, the coarse representation of the SSEM does not perform well across the full range of grazing profile widths. Overall, we find that as the grazing profile width increases, the RMS error between the SSEM and the ROEM decreases by several orders of magnitude in phytoplankton biomass (figure not shown).

In Fig. 10 we perform a similar comparison between the SSEM and ROEM in 1D. We compare the depth structure of the biomass in each size class in the ROEM with that of the total biomass in each peak in the SSEM. Overall the behavior of the SSEM in 1D is well represented by the ROEM, although some discrepancies remain. Specifically, the large size classes at grazing profile widths of $\Delta\ell = 0.2\log_{10}$ (μm) and $0.3\log_{10}$ (μm) are less well captured by the ROEM, indicating some limitations with the choice of using a single size class in representing each biomass peak. Furthermore, the SSEM has slightly larger total biomass compared to the ROEM. Despite these discrepancies between the two models in 1D, the ROEM may still be preferable for ecosystem modeling applications due to its greatly reduced computational cost.

6. Discussion and conclusions

In this study, we find that quantization in biomass along the size spectrum as a consequence of top-down control in the form of grazing. Our model suggests an important role for prey-selectivity behavior, which has been identified as a grazing mechanism in laboratory studies of zooplankton and phytoplankton interactions (Hansen et al., 1994). However, comprehensive measurements of selective predation have not been conducted in *in-situ* environments. Perhaps the most compelling studying showing *in-situ* quantization in biomass was Schartau et al. (2010). They found that not only were phytoplankton quantized after a nutrient fertilization event in the IronExII campaign, but the biomass of their predators was also quantized along the size spectra. Observational studies have shown the emergence of dominant size classes reminiscent of quantization in productive regions of the global ocean (i.e. Eastern Boundary Upwelling Systems) that have high nutrient availability and support large plankton cells (Hood et al., 1991; Jonasz and Fournier, 1996; Zubkov et al., 2000; Worden et al., 2004; Schartau et al., 2010; Huete-Ortega et al., 2014). However, understanding environmental controls on quantization in the field can be difficult because of the variety of ecosystem processes involved.

In models, grazing is an important factor in setting the internal ecosystem dynamics (Ingrid et al., 1996; Venrick, 1982; Leibold, 1996; Fuchs and Franks, 2010). The functional representation of grazing is a determining factor in ecosystem models (Steele and Henderson, 1992; Chenillat et al., 2021), for example affecting population stability (Strom and Loukos, 1998), and driving quantization (Banas, 2011). Often, the

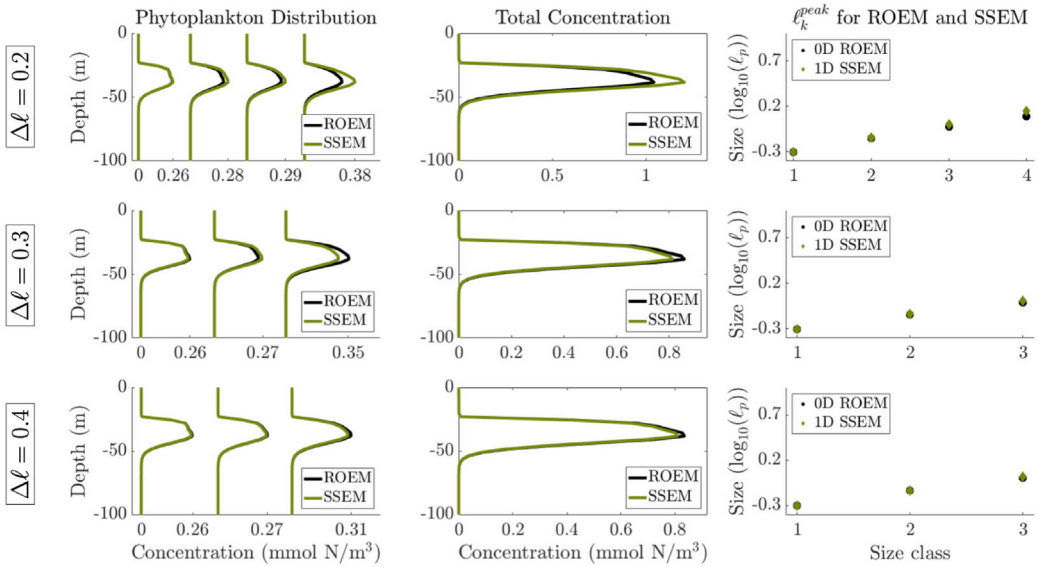

Fig. 10. A figure showing the solutions for phytoplankton SSEM (green), peaks integrated, and the ROEM (black), integrated for 100 years (left column), the total concentration (center column), and the concentration-weighted average size from the 1D SSEM and 0D-informed ROEM (right column). The restoring nutrient profile is configured to represent an oligotrophic surface ocean.

choice of zooplankton mortality closure is considered an important discriminant in setting internal ecosystem dynamics (Record et al., 2014). The choice of linear versus quadratic mortality in our model does not affect the quantization of biomass. Instead, a linear closure term in both phytoplankton and zooplankton allows for larger sizes classes to emerge, following a relationship set by the grazing profile width, but does not influence the location of the peaks (not shown). We note that the mortality formulation in between linear and quadratic mortality have been proposed (Record et al., 2014). Our tests with both linear and quadratic mortality suggest that these intermediate formulations would likely not alter the emergence of quantization however, a more systematic analysis of the effect of mortality is left to future work.

We show that the locations (in size space) of the biomass peaks is sensitive to the width of the grazing profile, $\Delta\ell$, which is the first order control on setting the behavior at steady state (see Fig. 6 and Banas (2011)). We find an approximately linear relationship between the width of the grazing profile and the distance between biomass peaks in both phytoplankton and zooplankton. This relationship loses explanatory power near bifurcation points in $\Delta\ell$-space. Successive bifurcations suggest that phytoplankton optimize their size based predominantly on grazing pressures, although explicitly showing this behavior is much more challenging. A caveat of our analysis is that the model exhibits non-linear behavior that is difficult to isolate from first principles.

Total nutrient availability and supply are secondary contributors to the distribution of modes along the size spectra. Large and intermediate size classes are responsible for a large fraction of the phytoplankton biomass at high nutrient forcing, while small phytoplankton contribute to most of the biomass at low nutrient forcing. This is consistent with other models and observations (Partensky et al., 1999; Zhou and Huntley, 1997; Sheldon et al., 1972; Hood et al., 1991; Huete-Ortega et al., 2014; Jonasz and Fournier, 1996). While changes in nutrient forcing leave the locations of the biomass peaks in size space approximately unchanged, increased nutrient forcing does result in emergence of larger size classes with spacing predicted by the grazing profile width. Qualitatively, we can describe this behavior as a mechanism to balance grazing pressures and nutrient uptake limitations. This mechanism in phytoplankton niche-filling has been studied by Leibold (1996), Ingrid et al. (1996), and Fuchs and Franks (2010), which show that large phytoplankton often outpace growth compared to their grazers by their cell size. For our reference solution, we chose a relatively broad grazing profile that is sufficiently far away from bifurcation points. While smaller grazing profile widths are perhaps more plausible (Hansen et al., 1994), they would not alter the model behavior, besides allowing a larger number of size peaks. The small width and high sharpness of the biomass peaks as the model approaches equilibrium are also rather unrealistic compared to broader distributions from *in-situ* studies (Schartau et al., 2010). Natural marine environments with horizontally variable nutrient availability and transport may smooth sharp points in the biomass spectra. Furthermore, we only investigate size as the axis of variability, while many more traits can be identified in natural plankton populations.

In general, quantization appears to be a robust feature of marine ecosystems, and ecosystem models, assuming some degree of competition for resources by the represented ecosystem components (here, size classes). Evolutionary models that focus on niche selection and emergent traits often show biomass peaks along their respective trait spectra (Loeuille and Loreau, 2004, 2005; Brännström et al., 2011; Sauterey et al., 2017; Edwards et al., 2018). In their study, Loeuille and Loreau (2005) note that quantization of biomass can be described as a method of niche selection for a given trait as a consequence of resource competition. In our model, as $\Delta\ell$ increases, zooplankton are able to graze a larger number of phytoplankton size classes, increasing resource competition. This, in effect, gives more zooplankton sizes access to the same resources (see Fig. 7). As a result of this increased competition, the total number of peaks in phytoplankton and zooplankton biomass decreases, and the preferential sizes are spread further in size space. Another way to induce changes in resource competition is size-grid resolution. At low size-grid resolution, zooplankton biomass shifts toward smaller size classes (see Fig. 3), while the total concentration in phytoplankton peaks remains approximately constant with respect to resolution in size space. This effect increases resource competition at smaller zooplankton sizes, due to the increase of biomass in those peaks.

With this set of experiments, we seek to provide insights into the behavior of the ecosystem as it relates to the emergence of peaks in size distribution. The behavior of the model can be summarized in the context of bottom-up and top-down controls. While there is some evidence of size quantization in observational studies (Hood et al., 1991; Schartau et al., 2010), there is not global evidence that specific quantization, like the solutions we present in this paper, is consistently present across diverse ocean conditions. An outcome of this study is to enable deeper understanding of the behavior of quantization in regions

of the ocean where it occurs. For example, if a region has quantized biomass with a few distinct peaks, and a large average size, one may hypothesize that zooplankton preferentially graze on many size classes. Alternatively, if there are many size classes with a small average size, one may hypothesize that zooplankton prefer to graze a few particular sizes.

A practical application of this study extended to other general marine ecosystem models with robust quantization is to use the same method of model complexity reduction we used to derive the ROEM, *i.e.* to simulate only the subset of organismal classes corresponding to dominant peaks in trait space. The primary assumptions used to define the ROEM are that biomass peaks are infinitesimally narrow and that their locations in size space are insensitive to environmental conditions. We note that biomass quantization collapses to a continuous spectra once we restrict one predator to only graze one prey, i.e., when grazing becomes extremely selective (Poulin and Franks, 2010). Thus, the representational capacity of the ROEM falls with very selective grazing.

Our solutions show that the total biomass in the SSEM is represented by the ROEM to a good degree of approximation. However, there remain some issues with over-estimation of total biomass for large zooplankton in 0D with highly selective grazing, and issues with the under-estimation of large phytoplankton biomass in 1D. Although the ROEM does not always have high accuracy in representation of the peaks, overall, we find that as the distance between peaks becomes comparable to the width of the grazing profile the reduced model exhibits increased performance and accuracy. However this issue exists in all size structured ecosystem models that are coarsely discretized (see Fig. 3). These issues have not be investigated in detail in this study. However, there are implications for the representation of the ecosystem, and specifically the biomass of grazers if large plankton are over or underestimated (Cyr and Pace, 1992; Chenillat et al., 2021).

As a part of the development of the ROEM, we assume that the biomass in each peak can be effectively represented as a delta function in size space; however this is not a realistic assumption for phytoplankton sizes. For example, plankton morphology can change over a cell's lifetime, or across an even limited number of generations, allowing phytoplankton growth as a mechanism of niche adaptation. In order to more accurately resolve the predicted biomass peaks, future studies could allow for more stable solutions by picking a small window, inside of the predicted location of each peak, and resolving a few points within the boundaries of the peak. Additional approaches could also include representing each peaks as a Gaussian function with a fixed width, or including more points near the estimated concentration-weighted size. However, these methods have not been tested.

The most relevant application of the model complexity reduction in the ROEM would be to use in Earth System Models where vertical and horizontal resolution limit the number of biogeochemical tracers due to computational constraints. Ultimately, sharp biomass peaks emerge under constant nutrient forcing over long timescales, but would likely be smoothed out with more dimensions of physical variability and coarser size-grid resolution (e.g., Ward et al. (2012)). This likely would affect the accuracy of the ROEM because of the assumption that each mode can be represented as a relatively narrow peak. We suggest that a possible way to address inaccuracies in the representation of the SSEM by the ROEM is to representing each biomass peak as a resolved interval along the size-grid instead of a single point.

A major benefit of this approach is to resolve an entire high-resolution ecosystem model with a few, emergent modes. The strategy presented in this study to capture ecosystem dynamics in a reduced order model can be extended to a variety of traits that results in robust quantization of biomass. We expect quantization in the SSEM due to size-selectivity in the grazing profile; however, the functionality and accuracy of ROEM in higher dimensions is yet to be explored. Future work with the ROEM is to test the accuracy of the model in horizontally heterogeneous environments, and compare to quantization in the SSEM. Coupling the ROEM to more comprehensive 2D and 3D models, allows more extensive investigations of the planktonic food-web in a computationally efficient framework.

CRediT authorship contribution statement

Jordyn E. Moscoso: Coordinated the development of the size structured ecosystem model, Developed and implemented the zero and one dimensional ecosystem model, Fine tuned the size diffusion, Further ecosystem testing and model development, Prepared the manuscript. **Daniele Bianchi:** Coordinated the development of the reduced order ecosystem model, model testing, model evaulation, and further assisted in the preparation of the manuscript.. **Andrew L. Stewart:** Coordinated the development of the reduced order ecosystem model, model testing, model evaulation, and further assisted in the preparation of the manuscript.

Declaration of competing interest

The authors declare that they have no known competing financial interests or personal relationships that could have appeared to influence the work reported in this paper.

Acknowledgments

The authors acknowledge resources from the Extreme Science and Engineering Discovery Environment (XSEDE, Towns et al., 2014), which is supported by National Science Foundation, United States grant number ACI-1548562. D.B. acknowledges support from NOAA, United States under Ecosystem and Harmful Algal Bloom (ECOHAB) Award NA18NOS4780174, and the Alfred P. Sloan Foundation, United States. Without implying their endorsement, the authors would also like to thank Ben Ward, Naomi Levine, and Jim McWilliams for helpful conversations. The authors would also like to thank Neil Banas, and an anonymous reviewer for their helpful comments and suggestions which made the presentation of this study more clear.

References

Adjou, M., Bendtsen, J., Richardson, K., 2012. Modeling the influence from ocean transport, mixing and grazing on phytoplankton diversity. Ecol. Model. 225, 19–27.

Andersen, K., Berge, T., Goncalves, R., Hartvig, M., Heuschele, J., Hylander, S., Jacobsen, N., Lindemann, C., Martens, E., Neuheimer, A., Olsson, K., Palacz, A., Prowe, A., Sainmont, J., Traving, S., Visser, A., Wadhwa, N., Kiorboe, T., 2016. Characteristic sizes of life in the oceans, from bacteria to whales. Annu. Rev. Mar. Sci. 8 (1), 217–241.

Armstrong, R.A., 1994. Grazing limitation and nutrient limitation in marine ecosystems: steady state solutions of an ecosystem model with multiple food chains. Limnol. Oceanogr. 39 (3), 597–608.

Armstrong, R.A., McGehee, R., 1980. Competitive exclusion. Amer. Nat. 115 (2), 151–170.

Banas, N.S., 2011. Adding complex trophic interactions to a size-spectral plankton model: Emergent diversity patterns and limits on predictability. Ecol. Model. 222, 2663–2675.

Banse, K., 1994. Uptake of inorganic carbon and nitrate by marine plankton and the redfield ratio. Glob. Biogeochem. Cycles 8 (1), 81–84.

Barton, A.D., Dutkiewicz, S., Flierl, G., Bragg, J., Follows, M.J., 2010. Patterns of diversity in marine phytoplankton. Science 327 (5972), 1509–1511.

Beckmann, A., Hense, I., 2007. Beneath the surface: Characteristics of oceanic ecosystems under weak mixing conditions–a theoretical investigation. Prog. Oceanogr. 75 (4), 771–796.

Behrenfeld, M.J., Boss, E.S., 2014. Resurrecting the ecological underpinnings of ocean plankton blooms. Annu. Rev..

Boyd, P.W., Claustre, H., Levy, M., Siegel, D.A., Weber, T., 2019. Multi-faceted particle pumps drive carbon sequestration in the ocean. Nature 568 (7752), 327–335.

Brännström, Å., Loeuille, N., Loreau, M., Dieckmann, U., 2011. Emergence and maintenance of biodiversity in an evolutionary food-web model. Theor. Ecol. 4 (4), 467–478.

Bruggeman, J., Kooijman, S.A., 2007. A biodiversity-inspired approach to aquatic ecosystem modeling. Limnol. Oceanogr. 52 (4), 1533–1544.

Cael, B., Cavan, E.L., Britten, G.L., 2021. Reconciling the size-dependence of marine particle sinking speed. Geophys. Res. Lett. 48 (5), e2020GL091771.

Cavender-Bares, K.K., Rinaldo, A., Chisholm, S.W., 2001. Microbial size spectra from natural and nutrient enriched ecosystems. Limnol. Oceanogr. 46 (4), 778–789.

Chavez, F.P., 1989. Size distribution of phytoplankton in the central and eastern tropical Pacific. Glob. Biogeochem. Cycles 3 (1), 27–35.

Chenillat, F., Rivière, P., Capet, X., Franks, P.J., Blanke, B., 2013. California coastal upwelling onset variability: cross-shore and bottom-up propagation in the planktonic ecosystem. PLoS One 8 (5), e62281.
Chenillat, F., Rivière, P., Ohman, M.D., 2021. On the sensitivity of plankton ecosystem models to the formulation of zooplankton grazing. PLoS One 16 (5), e0252033.
Chisholm, S.W., 1992. Phytoplankton size. In: Primary Productivity and Biogeochemical Cycles in the Sea. Springer, pp. 213–237.
Cullen, J.J., 1982. The deep chlorophyll maximum: comparing vertical profiles of chlorophyll a. Can. J. Fish. Aquat. Sci. 39 (5), 791–803.
Cyr, H., Pace, M.L., 1992. Grazing by zooplankton and its relationship to community structure. Can. J. Fish. Aquat. Sci. 49 (7), 1455–1465.
Deser, C., Timlin, M.S., 1997. Atmosphere–ocean interaction on weekly timescales in the North Atlantic and Pacific. J. Clim. 10 (3), 393–408.
Ducklow, H.W., Steinberg, D.K., Buesseler, K.O., 2001. Upper ocean carbon export and the biological pump. Oceanography 14 (4), 50–58.
Dunne, J.P., Armstrong, R.A., Gnanadesikan, A., Sarmiento, J.L., 2005. Empirical and mechanistic models for the particle export ratio. Glob. Biogeochem. Cycles 19 (4).
Dutkiewicz, S., Cermeno, P., Jahn, O., Follows, M.J., Hickman, A.E., Taniguchi, D.A., Ward, B.A., 2020. Dimensions of marine phytoplankton diversity. Biogeosciences 17 (3), 609–634.
Dutkiewicz, S., Follows, M.J., Bragg, J.G., 2009. Modeling the coupling of ocean ecology and biogeochemistry. Glob. Biogeochem. Cycles 23 (4).
Dutkiewicz, S., Ward, B., Monteiro, F., Follows, M., 2012. Interconnection of nitrogen fixers and iron in the Pacific ocean: Theory and numerical simulations. Glob. Biogeochem. Cycles 26 (1).
Edwards, K.F., Kremer, C.T., Miller, E.T., Osmond, M.M., Litchman, E., Klausmeier, C.A., 2018. Evolutionarily stable communities: a framework for understanding the role of trait evolution in the maintenance of diversity. Ecol. Lett. 21 (12), 1853–1868.
Edwards, K.F., Thomas, M.K., Klausmeier, C.A., Litchman, E., 2012. Allometric scaling and taxonomic variation in nutrient utilization traits and maximum growth rate of phytoplankton. Limnol. Oceanogr. 57 (2), 554–566.
Eppley, R., Rogers, J., McCarthy, J., 1969. Half-saturation constants for uptake of nitrate and ammonium by marine phytoplankton. Limnol. Oceanogr. 17, 912—920.
Follows, M.J., Dutkiewicz, S., 2011. Modeling diverse communities of marine microbes. Annu. Rev. Mar. Sci. 3, 427–451.
Follows, M.J., Dutkiewicz, S., Grant, S., Chisholm, S.W., 2007. Emergent biogeography of microbial communities in a model ocean. Science 315 (5820), 1843–1846.
Fowler, B.L., Neubert, M.G., Hunter-Cevera, K.R., Olson, R.J., Shalapyonok, A., Solow, A.R., Sosik, H.M., 2020. Dynamics and functional diversity of the smallest phytoplankton on the northeast US shelf. Proc. Natl. Acad. Sci. 117 (22), 12215–12221.
Franks, P.J., 2002. NPZ models of plankton dynamics: their construction, coupling to physics, and application. J. Oceanogr. 58 (2), 379–387.
Fuchs, H.L., Franks, P.J., 2010. Plankton community properties determined by nutrients and size-selective feeding. Mar. Ecol. Prog. Ser. 413, 1–15.
Gentleman, W., Leising, A., Frost, B., Strom, S., Murray, J., 2003. Functional responses for zooplankton feeding on multiple resources: a review of assumptions and biological dynamics. Deep Sea Res. II 50 (22–26), 2847–2875.
Giometto, A., Altermatt, F., Carrara, F., Maritan, A., Rinaldo, A., 2013. Scaling body size fluctuations. Proc. Natl. Acad. Sci. 110 (12), 4646–4650.
Gregg, W.W., Casey, N.W., 2007. Modeling coccolithophores in the global oceans. Deep Sea Res. II 54 (5–7), 447–477.
Hales, B., Moum, J.N., Covert, P., Perlin, A., 2005. Irreversible nitrate fluxes due to turbulent mixing in a coastal upwelling system. J. Geophys. Res. Oceans 110 (C10).
Hansen, B., Bjornsen, P., Hansen, P., 1994. The size ratio between planktonic predators and their prey. Limnol. Oceanogr. 39, 395–403.
Henson, S.A., Cael, B., Allen, S.R., Dutkiewicz, S., 2021. Future phytoplankton diversity in a changing climate. Nature Commun. 12 (1), 1–8.
Hillebrand, H., Azovsky, A.I., 2001. Body size determines the strength of the latitudinal diversity gradient. Ecography 24 (3), 251–256.
Hood, R.R., Abbott, M.R., Huyer, A., 1991. Phytoplankton and photosynthetic light response in the coastal transition zone off northern California in June 1987. J. Geophys. Res. Oceans 96 (C8), 14769–14780.
Hood, R.R., Laws, E.A., Armstrong, R.A., Bates, N.R., Brown, C.W., Carlson, C.A., Chai, F., Doney, S.C., Falkowski, P.G., Feely, R.A., et al., 2006. Pelagic functional group modeling: Progress, challenges and prospects. Deep Sea Res. II 53 (5–7), 459–512.
Huete-Ortega, M., Rodríguez-Ramos, T., López-Sandoval, D., Cermeño, P., Blanco, J.M., Palomino, R.L., Rodríguez, J., Marañón, E., 2014. Distinct patterns in the size-scaling of abundance and metabolism in coastal and open-ocean phytoplankton communities. Mar. Ecol. Prog. Ser. 515, 61–71.
Huisman, J., van Oostveen, P., Weissing, F.J., 1999. Critical depth and critical turbulence: two different mechanisms for the development of phytoplankton blooms. Limnol. Oceanogr. 44 (7), 1781–1787.
Huisman, J., Weissing, F.J., 2001. Fundamental unpredictability in multispecies competition. Amer. Nat. 157 (5), 488–494.
Hutchinson, G.E., 1961. The paradox of the plankton. Amer. Nat. 95 (882), 137–145.
Ingrid, G., Andersen, T., Vadstein, O., 1996. Pelagic food webs and eutrophication of coastal waters: impact of grazers on algal communities. Mar. Pollut. Bull. 33 (1–6), 22–35.
Iversen, M.H., Lampitt, R.S., 2020. Size does not matter after all: No evidence for a size-sinking relationship for marine snow. Prog. Oceanogr. 189, 102445.
Johnson, K.S., Riser, S.C., Karl, D.M., 2010. Nitrate supply from deep to near-surface waters of the North Pacific subtropical gyre. Nature 465 (7301), 1062–1065.
Jonasz, M., Fournier, G., 1996. Approximation of the size distribution of marine particles by a sum of log-normal functions. Limnol. Oceanogr. 41 (4), 744–754.
Karp-Boss, L., Azevedo, L., Boss, E., 2007. LISST-100 measurements of phytoplankton size distribution: Evaluation of the effects of cell shape. Limno. Oceanogr. Methods 5 (11), 396–406.
Kiørboe, T., 2011. How zooplankton feed: mechanisms, traits and trade-offs. Biol. Rev. 86 (2), 311–339.
Klausmeier, C.A., Kremer, C.T., Koffel, T., 2020. Trait-based ecological and eco-evolutionary theory. In: Theoretical Ecology. Oxford University Press, pp. 161–194.
Klausmeier, C.A., Litchman, E., 2001. Algal games: The vertical distribution of phytoplankton in poorly mixed water columns. Limnol. Oceanogr. 46 (8), 1998–2007.
Large, W.G., McWilliams, J.C., Doney, S.C., 1994. Oceanic vertical mixing: A review and a model with a nonlocal boundary layer parameterization. Rev. Geophys. 32 (4), 363–403.
Lehman, J.T., 1991. Interacting growth and loss rates: The balance of top-down and bottom-up controls in plankton communities. Limnol. Oceanogr. 36 (8), 1546–1554.
Leibold, M.A., 1996. A graphical model of keystone predators in food webs: trophic regulation of abundance, incidence, and diversity patterns in communities. Amer. Nat. 147 (5), 784–812.
Lévy, M., 2003. Mesoscale variability of phytoplankton and of new production: Impact of the large-scale nutrient distribution. J. Geophys. Res. Oceans 108 (C11).
Lévy, M., Jahn, O., Dutkiewicz, S., Follows, M.J., 2014. Phytoplankton diversity and community structure affected by oceanic dispersal and mesoscale turbulence. Limnol. Oceanogr. Fluids Environ. 4 (1), 67–84.
Lévy, M., Klein, P., Treguier, A.-M., 2001. Impact of sub-mesoscale physics on production and subduction of phytoplankton in an oligotrophic regime. J. Mar. Res. 59 (4), 535–565.
Litchman, E., Klausmeier, C.A., Schofield, O.M., Falkowski, P.G., 2007. The role of functional traits and trade-offs in structuring phytoplankton communities: scaling from cellular to ecosystem level. Ecol. Lett. 10 (12), 1170–1181.
Loeuille, N., Loreau, M., 2004. Nutrient enrichment and food chains: can evolution buffer top-down control? Theor. Popul. Biol. 65 (3), 285–298.
Loeuille, N., Loreau, M., 2005. Evolutionary emergence of size-structured food webs. Proc. Natl. Acad. Sci. 102 (16), 5761–5766.
Mahadevan, A., D'asaro, E., Lee, C., Perry, M.J., 2012. Eddy-driven stratification initiates North Atlantic spring phytoplankton blooms. Science 337 (6090), 54–58.
Mayzaud, P., Poulet, S.A., 1978. The importance of the time factor in the response of zooplankton to varying concentrations of naturally occurring particulate matter 1. Limnol. Oceanogr. 23 (6), 1144–1154.
McCave, I., 1975. Vertical flux of particles in the ocean. Deep Sea Res. Oceanogr. Abstracts 22 (7), 491–502.
McClatchie, S., 2016. Regional Fisheries Oceanography of the California Current System. Springer.
McQueen, D.J., Post, J.R., Mills, E.L., 1986. Trophic relationships in freshwater pelagic ecosystems. Can. J. Fish. Aquat. Sci. 43 (8), 1571–1581.
Merico, A., Brandt, G., Smith, S.L., Oliver, M., 2014. Sustaining diversity in trait-based models of phytoplankton communities. Front. Ecol. Evol. 2, 59.
Messié, M., Ledesma, J., Kolber, D.D., Michisaki, R.P., Foley, D.G., Chavez, F.P., 2009. Potential new production estimates in four eastern boundary upwelling ecosystems. Prog. Oceanogr. 83 (1–4), 151–158.
Moloney, C.L., Field, J.G., 1991. The size-based dynamics of plankton food webs. I. A simulation model of carbon and nitrogen flows. J. Plankton Res. 13 (5), 1003–1038.
Moore, J., Doney, S.C., Kleypas, J.A., Glover, D.M., Fung, I.Y., 2001. An intermediate complexity marine ecosystem model for the global domain. Deep Sea Res. 49 (1), 403–462.
Moscoso, J.E., Stewart, A.L., Bianchi, D., McWilliams, J.C., 2021. The meridionally averaged model of eastern boundary upwelling systems (MAMEBUSv1. 0). Geosci. Model Dev. 14 (2), 763–794.
Mousing, E.A., Richardson, K., Bendtsen, J., Cetinić, I., Perry, M.J., 2016. Evidence of small-scale spatial structuring of phytoplankton alpha-and beta-diversity in the open ocean. J. Ecology 104 (6), 1682–1695.
Murray, A., Parslow, J., 1999. The analysis of alternative formulations in a simple model of a coastal ecosystem. Ecol. Model. 119 (2–3), 149–166.
Obata, A., Ishizaka, J., Endoh, M., 1996. Global verification of critical depth theory for phytoplankton bloom with climatological in situ temperature and satellite ocean color data. J. Geophys. Res. Oceans 101 (C9), 20657–20667.
Partensky, F., Blanchot, J., Vaulot, D., 1999. Differential distribution and ecology of prochlorococcus and synechococcus in oceanic waters: a review. Bull.-Inst. Oceanogr. Monaco-Numer. Special- 457–476.
Poulin, F.J., Franks, P.J., 2010. Size-structured planktonic ecosystems: constraints, controls and assembly instructions. J. Plankton Res. 32 (8), 1121–1130.
Quere, C.L., Harrison, S.P., Colin Prentice, I., Buitenhuis, E.T., Aumont, O., Bopp, L., Claustre, H., Cotrim Da Cunha, L., Geider, R., Giraud, X., et al., 2005. Ecosystem dynamics based on plankton functional types for global ocean biogeochemistry models. Global Change Biol. 11 (11), 2016–2040.

Record, N.R., Pershing, A.J., Maps, F., 2014. The paradox of the "paradox of the plankton". ICES J. Mar. Sci. 71 (2), 236–240.
Richardson, T.L., Jackson, G.A., 2007. Small phytoplankton and carbon export from the surface ocean. Science 315 (5813), 838–840.
Righetti, D., Vogt, M., Gruber, N., Psomas, A., Zimmermann, N.E., 2019. Global pattern of phytoplankton diversity driven by temperature and environmental variability. Sci. Adv. 5 (5), eaau6253.
Rodriguez, J., Tintoré, J., Allen, J.T., Blanco, J.M., Gomis, D., Reul, A., Ruiz, J., Rodríguez, V., Echevarría, F., Jiménez-Gómez, F., 2001. Mesoscale vertical motion and the size structure of phytoplankton in the ocean. Nature 410 (6826), 360–363.
Ryabov, A.B., Rudolf, L., Blasius, B., 2010. Vertical distribution and composition of phytoplankton under the influence of an upper mixed layer. J. Theoret. Biol. 263 (1), 120–133.
Sarmiento, J.L., Gruber, N., 2006. Ocean Biogeochemical Dynamics. Princeton University Press.
Sauterey, B., Ward, B., Rault, J., Bowler, C., Claessen, D., 2017. The implications of eco-evolutionary processes for the emergence of marine plankton community biogeography. Amer. Nat. 190 (1), 116–130.
Schartau, M., Landry, M.R., Armstrong, R.A., 2010. Density estimation of plankton size spectra: a reanalysis of IronEx II data. J. Plankton Res. 32 (8), 1167–1184.
Sheldon, R., Prakash, A., Sutcliffe, Jr., W., 1972. The size distribution of particles in the ocean 1. Limnol. Oceanogr. 17 (3), 327–340.
Sommer, U., 1989. The role of competition for resources in phytoplankton succession. In: Plankton Ecology. Springer, pp. 57–106.
Steele, J.H., Henderson, E.W., 1992. The role of predation in plankton models. J. Plankton Res. 14 (1), 157–172.
Stock, C.A., John, J.G., Rykaczewski, R.R., Asch, R.G., Cheung, W.W., Dunne, J.P., Friedland, K.D., Lam, V.W., Sarmiento, J.L., Watson, R.A., 2017. Reconciling fisheries catch and ocean productivity. Proc. Natl. Acad. Sci. 114 (8), E1441–E1449.
Strom, S.L., Loukos, H., 1998. Selective feeding by protozoa: model and experimental behaviors and their consequences for population stability. J. Plankton Res. 20 (5), 831–846.
Sverdrup, H., 1953. On conditions for the vernal blooming of phytoplankton. J. Cons. Int. Explor. Mer 18 (3), 287–295.
Tang, E., 1995. The allometry of algal growth rates. J. Plankton Res. 17, 1325–1335.
Terseleer, N., Bruggeman, J., Lancelot, C., Gypens, N., 2014. Trait-based representation of diatom functional diversity in a plankton functional type model of the eutrophied southern North sea. Limnol. Oceanogr. 59 (6), 1958–1972.
Towns, J., Cockerill, T., Dahan, M., Foster, I., Gaither, K., Grimshaw, A., Hazlewood, V., Lathrop, S., Lifka, D., Peterson, G.D., Roskies, R., Scott, J.R., Wilkins-Diehr, N., 2014. XSEDE: Accelerating scientific discovery. Comput. Sci. Eng. (ISSN: 1521-9615) 16 (5), 62–74. http://dx.doi.org/10.1109/MCSE.2014.80.
Tréguer, P., Bowler, C., Moriceau, B., Dutkiewicz, S., Gehlen, M., Aumont, O., Bittner, L., Dugdale, R., Finkel, Z., Iudicone, D., et al., 2018. Influence of diatom diversity on the ocean biological carbon pump. Nat. Geosci. 11 (1), 27–37.
Vallina, S.M., Follows, M., Dutkiewicz, S., Montoya, J.M., Cermeno, P., Loreau, M., 2014. Global relationship between phytoplankton diversity and productivity in the ocean. Nature Commun. 5 (1), 1–10.
Venrick, E., 1982. Phytoplankton in an oligotrophic ocean: Observations and questions: Ecological archives M052-002. Ecol. Monograph 52 (2), 129–154.
Venrick, E., 1993. Phytoplankton seasonality in the central North Pacific: the endless summer reconsidered. Limnol. Oceanogr. 38 (6), 1135–1149.
Venrick, E., 2002. Floral patterns in the California current system off southern California: 1990–1996. J. Mar. Res. 60 (1), 171–189.
Verity, P.G., Smetacek, V., 1996. Organism life cycles, predation, and the structure of marine pelagic ecosystems. Mar. Ecol. Prog. Ser. 130, 277–293.
Ward, B.A., Dutkiewicz, S., Follows, M.J., 2014. Modelling spatial and temporal patterns in size-structured marine plankton communities: top–down and bottom–up controls. J. Plankton Res. 36 (1), 31–47.
Ward, B.A., Dutkiewicz, S., Jahn, O., Follows, M.J., 2012. A size-structured food-web model for the global ocean. Luminol. Oceanogr. 57 (6), 1877–1891.
Whitney, F., Wong, C., Boyd, P., 1998. Interannual variability in nitrate supply to surface waters of the Northeast Pacific ocean. Mar. Ecol. Prog. Ser. 170, 15–23.
Worden, A.Z., Nolan, J.K., Palenik, B., 2004. Assessing the dynamics and ecology of marine picophytoplankton: the importance of the eukaryotic component. Limnol. Oceanogr. 49 (1), 168–179.
Zhou, M., Huntley, M.E., 1997. Population dynamics theory of plankton based on biomass spectra. Mar. Ecol. Prog. Ser. 159, 61–73.
Zubkov, M.V., Sleigh, M.A., Burkill, P.H., 2000. Assaying picoplankton distribution by flow cytometry of underway samples collected along a meridional transect across the atlantic ocean. Aquat. Microb. Ecol. 21 (1), 13–20.